

Universitat Politècnica de Catalunya
Facultat de Matemàtiques i Estadística

Degree in Mathematics
Bachelor's Degree Thesis

**Mathematical modeling and numerics
of opinion consensus
and polarization dynamics**

Bruno Fernández Carballo

Supervised by Gissell Estrada-Rodriguez
January, 2026

First of all, I would like to thank Gissell for the excellent guidance and mentorship provided during these months. I am also deeply grateful for her corrections and availability. She has not only helped me understand the difficult concepts presented in this thesis but has also given me advice for my future steps.

I am also grateful to my colleagues Jaume, Javi, and Bruno; they have been a fundamental and necessary part of this stage of my education.

Lastly, I want to thank my parents, Claudia and Albert, for always being there and supporting me in everything I do.

Abstract

This thesis investigates the application of the Boltzmann equation to opinion consensus and polarization dynamics. Building on classical kinetic gas theory, we examine opinion models that incorporate agent-specific variables, such as external diffusion and compromise propensity, to describe social interactions. To solve the governing equations, we develop and implement Direct Simulation Monte Carlo (DSMC) algorithms for the homogeneous Boltzmann equation. The numerical scheme is extensively studied and subsequently applied to simulate and analyze the proposed opinion dynamics.

Keywords

Kinetic equations, opinions, Monte Carlo methods.

Contents

1	Introduction	4
2	Derivation of Boltzmann equation	6
2.1	The microscopic approach and single-particle distribution function.	6
2.2	Derivation of the Boltzmann equation	8
2.3	From the linear Boltzmann equation to the heat equation	11
3	Kinetic equations for opinion dynamics	16
3.1	"Classical" opinion dynamics Boltzmann equation	16
3.2	Compromise and diffusion in opinions	20
4	Monte Carlo methods for kinetic equations	22
4.1	Preliminaries	22
4.2	Fundamental features and assumptions of DSMC	23
4.3	Mathematical tools for DSMC	24
4.3.1	The splitting approach	24
4.3.2	Random sampling techniques	25
4.3.3	The collision kernel	25
4.4	Direct simulation schemes	26
4.4.1	Nanbu-Babovsky's scheme	27
5	Numerical Experiment	29
5.1	The Kac equation	29
5.1.1	Normalization of the analytical solution	30
5.1.2	Asymptotics of the solution of the Kac equation	31
5.2	Numerical results	31
5.2.1	Quantitative comparison.	32
5.2.2	Influence of time discretization	33
5.2.3	Sensitivity and scaling of the parameter ε	34
6	Numerical Analysis : Opinion Dynamics	38
6.1	The kinetic model and interaction rules	38
6.2	Numerical implementation	39
6.3	Numerical results	40
6.3.1	Influence of bounded confidence (r)	40
6.3.2	Influence of noise (σ)	42

1. Introduction

The mathematical description of interacting particle systems constitutes one of the most fundamental pillars in modern physics. Originally developed in the late 19th century to describe the behavior of dilute gases, kinetic theory bridges the gap between the microscopic world, which is governed by the deterministic Newtonian trajectories of billions of atoms, and the macroscopic observable world described by gas properties such as volume, density or temperature. Central to this framework is the Boltzmann equation, derived by Ludwig Boltzmann in 1872, which describes the statistical evolution of a system, not by tracking every single particle, but by modeling the time evolution of a probability distribution function in phase space [9]. This equation is set at the mesoscopic level, an intermediate regime that connects microscopic and macroscopic levels.

While this theory was originally conceived for gases, lately it has begun to be applied in a field known as *sociophysics* [33]. Researchers realized that the mathematical background and tools used to describe gas kinetics can be effective when applied to multi-agent systems in other disciplines. The underlying logic is that, in a similar way to gases (that are composed of the order of 10^{23} molecules), human societies, biological colonies, and economic markets are formed by a large number of interacting agents. Although individual behavior is complex and often unpredictable, the collective dynamics of the system exhibit statistical regularities that can be modeled using kinetic equations [8]. This analogy has been successfully used in diverse fields: in biology, describing the collective swarming of bacteria or the flocking of birds [29]; in economics, where the exchange of wealth in a closed market is mathematically analogous to the conservation of energy in molecular collisions [11]; and in social sciences, to model the spread of culture, language, and opinions [27, 12].

To apply this framework appropriately, we must establish clear analogies between the physical and the modeled quantities. In a gas, the fundamental variable is the particle's velocity, and the system evolves through binary collisions that conserve momentum and energy. In the social models introduced below, the "velocity" corresponds to an agent's continuous opinion (or wealth in economic models), and a "collision" corresponds to a social interaction (or transaction) where agents update their states (opinions or wealth, respectively). Similarly, in biological swarming models, the "velocity" represents the actual direction of motion of the animal, while the interaction corresponds to a social alignment mechanism, where individuals adjust their path to match that of their neighbors [7].

The primary objective of this thesis is to apply the kinetic theory framework to the study of opinion dynamics. Specifically, we focus on the kinetic models proposed by Toscani [27], which consider opinions not as discrete choices (e.g., "Yes/No") but as continuous variables evolving within a bounded domain. In this context, a social interaction is modeled as a microscopic collision between two agents. These interactions are governed by two fundamental processes: compromise, where agents adjust their opinions to reduce the distance between each other, and diffusion, representing the stochastic influence of the environment. Furthermore, this model can be extended to incorporate other individual traits, such as conviction, leadership qualities, or assertiveness, allowing a broader description of social behavior. Then, by deriving the Boltzmann-type equations for these interactions, we can predict different macroscopic phenomena such as consensus, polarization into two opposing groups, or fragmentation into multiple isolated clusters.

The choice to use a kinetic description rather than a discrete one is driven by both computational and analytical considerations. While discrete models effectively track individual trajectories, they become computationally prohibitive and difficult to interpret as the population size N increases. In contrast, the kinetic approach, obtained in the limit as $N \rightarrow \infty$, offers a significant advantage by deriving evolution equations for the particle density. This framework allows for the analysis and characterization of macroscopic behaviors independently of the number of agents.

However, the resulting integro-differential equations are high-dimensional (evolving in time, physical space and velocity space) and non-linear, due to the collision operator. Consequently, analytical solutions are generally intractable. Furthermore, standard deterministic numerical methods, such as finite difference schemes, become computationally expensive as the dimension of the phase space grows. To address this, we employ numerical methods, specifically Monte Carlo simulations. In particular, we consider Direct Simulation Monte Carlo (DSMC) methods, which were originally developed for aerospace engineering to simulate rarefied gas dynamics [4]. Unlike other numerical approaches, these methods simulate the probabilistic evolution of the particle system directly, allowing us to efficiently recover the solution of the Boltzmann equation. In this work, we specifically implement and analyze the Nanbu-Babovsky scheme [1, 21].

The thesis is organized as follows. In Chapter 2, we provide the foundations of kinetic theory based on [14], formally deriving the Boltzmann equation from microscopic particle dynamics and describing how particles behave and interact. Chapter 3 introduces the specific kinetic models for opinion dynamics following [27], and presents a formal derivation of a Boltzmann-type equation for [13], exploring distinct interaction rules such as compromise and diffusion. Chapter 4 details the numerical implementation, describing the DSMC algorithms, specifically the Nanbu-Babovsky scheme, used to solve the system equations. Finally, in Chapters 5 and 6, we present the simulation results. Specifically, in Chapter 5 we validate our implementation by employing the analytical solution of the Kac equation [23]. In Chapter 6, we show the results for the opinion model presented in [12], analyzing the formation of polarization and consensus.

2. Derivation of Boltzmann equation

In this section, we will analyze how to pass from microscopic to macroscopic dynamics for a system of hard spheres that travel in a straight line between two elastic collisions. The main objective will be to derive the Boltzmann equation which is posed at the mesoscopic level. Particularly, in Section 2.1, the microscopic approach is presented and the one-particle distribution function for a system of hard-spheres is deduced. In Section 2.2 we formally derive the non-linear Boltzmann equation. Finally, Section 2.3 is devoted to deriving the heat equation from the linear Boltzmann equation, finally arriving to the macroscopic level of description.

2.1 The microscopic approach and single-particle distribution function.

We consider a system of N hard-spheres of diameter ϵ in the phase-space (positions + velocities) $\mathbb{T}^{dN} \times \mathbb{R}^{dN}$, where \mathbb{T}^d denotes the d -dimensional torus. The torus is chosen as the space for the position coordinates because it guarantees periodicity. We denote $x_i \in \mathbb{T}^d$ the position and $v_i \in \mathbb{R}^d$ the velocity of each particle for $i = 1, \dots, N$.

As mentioned before, we assume that particles move in straight lines with constant velocity between collisions

$$\frac{dx_i}{dt} = v_i, \quad \frac{dv_i}{dt} = 0 \quad \text{provided that} \quad |x_i(t) - x_j(t)| > \epsilon \quad \text{for } 1 \leq i \neq j \leq N. \quad (1)$$

We denote $v_i(t^+)$ and $v_j(t^+)$ the velocities after the collisions, and $v_i(t^-), v_j(t^-)$ the pre-collision velocities. In classical kinetic theory, interactions are modeled as elastic collisions [4]. This distinguishes them from inelastic collisions where kinetic energy is dissipated as heat or deformation. Since we assume energy conservation during collisions, we consider elastic ones, which satisfy:

$$v_i(t^-) + v_j(t^-) = v_i(t^+) + v_j(t^+), \quad (2)$$

$$|v_i(t^-)|^2 + |v_j(t^-)|^2 = |v_i(t^+)|^2 + |v_j(t^+)|^2, \quad (3)$$

where (2) describes the conservation of kinetic momentum, and (3) characterizes the conservation of kinetic energy, which are essential properties in gas dynamics. When there is a collision, particle velocities are modified following

$$\begin{aligned} v_i(t^+) &= v_i(t^-) + w^{i,j} \cdot (v_i(t^+) - v_j(t^-)) w^{i,j}, \\ v_j(t^+) &= v_j(t^-) - w^{i,j} \cdot (v_i(t^+) - v_j(t^-)) w^{i,j}, \end{aligned} \quad (4)$$

where $w^{i,j} := \frac{x_i - x_j}{|x_i - x_j|}$ is the normal vector from the center x_i to the center x_j , as illustrated in Figure 1.

Then, one can subtract the second equation from the first in (4), and taking into account that in elastic collisions the relative velocity after collisions is reflected with respect to the normal vector:

$$(v_i(t^+) - v_j(t^+)) \cdot w^{i,j} = -(v_i(t^-) - v_j(t^-)) \cdot w^{i,j},$$

and after rearranging terms, we write (4) as follows:

$$\begin{aligned} v_i(t^+) &= v_i(t^-) - w^{i,j} \cdot (v_i(t^-) - v_j(t^-)) w^{i,j} \\ v_j(t^+) &= v_j(t^-) + w^{i,j} \cdot (v_i(t^-) - v_j(t^-)) w^{i,j}. \end{aligned} \quad (5)$$

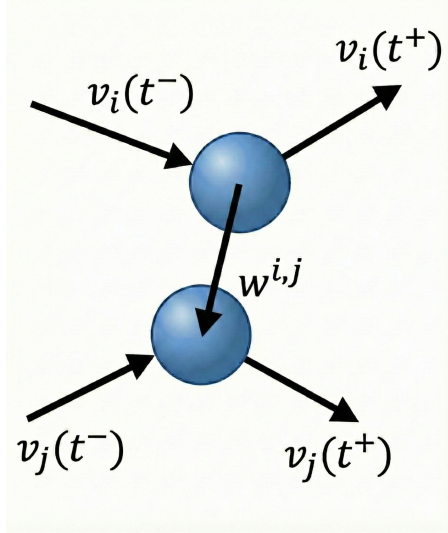


Figure 1: Schematic representation of an elastic collision. The unit vector $w^{i,j}$ connects the centers of the particles i and j . Adapted from [5].

To describe the system of N hard spheres, the N -particle distribution function $f_N(t, Z_N)$ is introduced, where $Z_N := (X_N, V_N)$ with $X_N = (x_1, \dots, x_N)$ and $V_N = (v_1, \dots, v_N)$ (i.e. the positions and velocities of all the N particles). Mathematically, the N -particle distribution function is defined as a non-negative Lebesgue-integrable function $f_N(t, \cdot) \in L^1(\mathbb{T}^{dN} \times \mathbb{R}^{dN})$ which satisfies

$$\int_{\mathbb{T}^{dN} \times \mathbb{R}^{dN}} f_N(t, Z_N) dZ_N = 1.$$

Consequently, the quantity $f_N(t, Z_N) dZ_N$ can be interpreted as the probability of finding the system at time t in the microscopic state where particle 1 has position x_1 and velocity v_1 , the particle 2, x_2 and v_2 , and so on. Particularly, this level of description is known as the microscopic level. Since the particles move freely between collisions following the trajectories defined in (1), and the system is conservative, the distribution function $f_N(t, Z_N)$ previously described satisfies the Liouville equation

$$\partial_t f_N + \sum_{i=1}^N v_i \cdot \nabla_{x_i} f_N = 0, \quad \forall (X_N, V_N) \in \mathcal{D}_N^\epsilon \times \mathbb{R}^{dN}, \quad (6)$$

with $\mathcal{D}_N^\epsilon := \{X_N \in \mathbb{T}^{dN}, \forall i \neq j, |x_i - x_j| > \epsilon\}$, and with a specular reflection in the boundary which represents a process where the relative velocity component perpendicular to the surface is reversed while the tangential component is preserved, ensuring the conservation of the system's energy. This stands in contrast to diffusive reflection, where particles are re-emitted in random directions independent of their incident velocity. Note that (6) describes the time evolution of the phase space distribution function. Also, notice that the Liouville equation is only valid in the domain \mathcal{D}_N^ϵ , which is the set of all possible physical configurations of particles where there are not two particles colliding.

Formally, this specular reflection condition is imposed on any particle pair (i, j) that is in contact, i.e. $|x_i - x_j| = \epsilon$, and on an approaching trajectory, specified by the condition $(v_i - v_j) \cdot (x_i - x_j) < 0$. Physically, this negative scalar product indicates that the particles are moving towards each other. Under this

condition, the probability density function is conserved across the collision boundary $\partial\mathcal{D}_N^\epsilon$, which can be written as

$$f_N(t, Z_N^{out}(i,j)) = f_N(t, Z_N^{in}(i,j)), \quad (7)$$

with $Z_N^{in}(i,j) := Z_N$, $X_N^{out}(i,j) := X_N$, $v_k^{out}(i,j) := v_k$ for all $k \in [1, N] \setminus \{i,j\}$, and using the rules of post-collisional velocities (5),

$$\begin{aligned} v_i^{out}(i,j) &= v_i^{in} - \frac{1}{\epsilon^2} (v_i^{in} - v_j^{in}) \cdot (x_i - x_j)(x_i - x_j) \\ v_j^{out}(i,j) &= v_j^{in} + \frac{1}{\epsilon^2} (v_i^{in} - v_j^{in}) \cdot (x_i - x_j)(x_i - x_j). \end{aligned}$$

Note that the scalar product $(v_i - v_j) \cdot (x_i - x_j)$ measures whether the particles are approaching or moving away from each other. If it is negative, it means that they are approaching and will collide.

To summarise, the reflection law is expressed as (7), which states that the probability density of the post-collision state, Z_N^{out} , is equal to the one of the pre-collision state, Z_N^{in} . The incoming state Z_N^{in} is defined as the system's state at the moment of impact, while the outgoing state, Z_N^{out} , is identical in all particle positions and velocities v_k of non-colliding particles ($k \neq i,j$). However, the velocities of the interacting particles are updated according to the collision laws (5).

Our aim is to study asymptotically the behavior of the first marginal of f_N , which can be defined as

$$f_N^{(1)}(t, z_1) := \int f_N(t, Z_N) dz_2 \dots dz_N. \quad (8)$$

Observe that it is the probability density of finding a particle in position x_1 and velocity v_1 in time t .

2.2 Derivation of the Boltzmann equation

Now, our objective is to formally derive the equation satisfied by $f_N^{(1)}$. To do so, it is necessary to establish the physical regime in which the macroscopic transport of particles and their microscopic collisions are of comparable magnitudes. This is achieved under the well-known *Boltzmann - Grad limit*. To understand this scaling, consider a particle that is travelling at velocity v during a time interval Δt . At the same time, suppose that there are N fixed particles, then, the moving particle will consider the other particles as cylinders of volume $\epsilon^{d-1}|v|\Delta t$, as illustrated in Figure 2. Since the cross-sectional area of the cylinder is proportional to ϵ^{d-1} , the total volume occupied by these potential interaction domains scales as $N\epsilon^{d-1}|v|\Delta t$.

For the probability of collision to remain significant, that is, of order 1, we must work under the Boltzmann-Grad limit. This scaling considers the asymptotic regime where $N \rightarrow \infty$ and $\epsilon \rightarrow 0$, such that the quantity $\alpha = N\epsilon^{d-1}$ remains finite. Under this condition, we identify α as the inverse of the mean free path ($l = 1/\alpha$). Physically α measures the frequency of collisions or the number of collisions per unit of distance while the mean free path l denotes the average distance that a particle travels before colliding with another. Observe that if the number of particles is large, the mean free path decreases, and as a consequence α increases; conversely, for a smaller number of particles, α decreases. Note that this limit is constructed precisely to keep this distance finite even as the particle diameter vanishes, allowing us to describe the macroscopic evolution of the system.

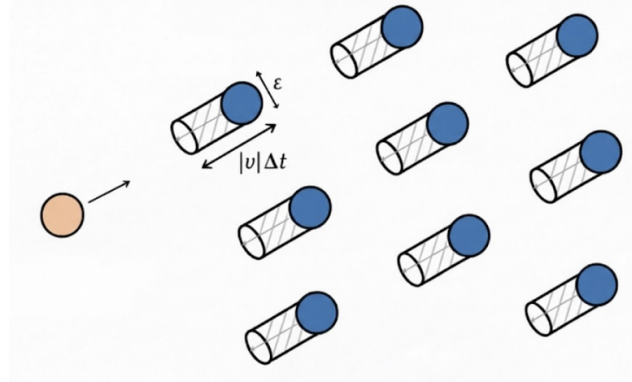


Figure 2: Collisional volume given by the cylinder.

Under this specific scaling, we integrate the Liouville equation (6) in the domain $\Omega := \mathcal{D}_N^\epsilon \times \mathbb{R}^{dN}$ except in $z_1 = (x_1, v_1)$, and we obtain:

$$\partial_t f_N^{(1)} + \int_{\Omega \setminus \{z_1\}} \sum_{i=1}^N v_i \cdot \nabla_{x_i} f_N dz_2 \dots dz_N = 0,$$

that can be simplified as

$$\partial_t f_N^{(1)} + v_1 \cdot \nabla_{x_1} f_N^{(1)} + \int_{\Omega \setminus \{z_1\}} \sum_{i=2}^N v_i \cdot \nabla_{x_i} f_N dz_2 \dots dz_N = 0. \quad (9)$$

Now, we focus in the third term of (9). Using the divergence theorem, we have

$$\sum_{i=2}^N \int_{\Omega \setminus \{z_1\}} v_i \cdot \nabla_{x_i} f_N dz_2 \dots dz_N = \sum_{i=2}^N \int_{|x_i - x_1|=\epsilon} f_N [(v_i - v_1) \cdot w_{i,1}] dz_2 \dots dz_N,$$

where $w_{i,1} = \frac{x_i - x_1}{|x_i - x_1|}$. Taking into account that $w_{i,1}$ is a unit vector and using the symmetry of f_N with respect to the variables, we get

$$\begin{aligned} & \sum_{i=2}^N \int_{|x_i - x_1|=\epsilon} f_N [(v_i - v_1) \cdot w_{i,1}] dz_2 \dots dz_N \\ &= (N-1)\epsilon^{d-1} \int_{\Omega \setminus \{z_1, z_2\}} \left(\int_{\mathbb{R}^d} \int_{x_2=x_1+\epsilon w} f_N(t, z_1, \dots, z_N) ((v_2 - v_1) \cdot w) dw dv_2 \right) dz_3 \dots dz_N, \end{aligned} \quad (10)$$

where $w = w_{2,1}$ and ϵ^{d-1} is the surface area scaling factor.

To simplify the integral term in (9), we first introduce the two-particle distribution function or second marginal of f_N as

$$f_N^{(2)}(t, z_1, z_2) = \int_{\Omega \setminus \{z_1, z_2\}} f_N(t, z_1, \dots, z_N) dz_3 \dots dz_N. \quad (11)$$

Next, we define the collisional operator $C_{1,2}$ that acts on $f_N^{(2)}$ which is given by

$$C_{1,2}f_N^{(2)} = \int_{\mathbb{R}^d} \int_{x_2=x_1+\epsilon w} f_N^{(2)}(t, x_1, v_1, x_2, v_2)((v_2 - v_1) \cdot w) dw dv_2. \quad (12)$$

Finally, using (11), (12) and the scaling relation $\alpha \approx (N-1)\epsilon^{d-1}$, we plug (10) into (9) to obtain

$$\partial_t f_N^{(1)} + v_1 \cdot \nabla_{x_1} f_N^{(1)} = \alpha \left(C_{1,2} f_N^{(2)} \right) \quad (13)$$

Now, defining the unit sphere

$$\mathbb{S}^{d-1} = \{w \in \mathbb{R}^d : \|w\| = 1\},$$

which consists of all unit vectors $w \in \mathbb{R}$, (12) can be rewritten in terms of the unit sphere to obtain

$$C_{1,2}f_N^{(2)} = \int_{\mathbb{R}^d} \int_{\mathbb{S}^{d-1}} f_N^{(2)}(t, x_1, v_1, x_1 + \epsilon w, v_2)((v_1 - v_2) \cdot w) dw dv_2.$$

Using the boundary conditions and (4), the integral can be split in two terms:

$$\begin{aligned} C_{1,2}f_N^{(2)} &= \int_{\mathbb{R}^d} \int_{\mathbb{S}_+^{d-1}} f_N^{(2)}(t, x_1, v'_1, x_1 + \epsilon w, v'_2)|((v_2 - v_1) \cdot w)| dw dv_2 \\ &\quad - \int_{\mathbb{R}^d} \int_{\mathbb{S}_-^{d-1}} f_N^{(2)}(t, x_1, v_1, x_1 + \epsilon w, v_2)|((v_1 - v_2) \cdot w)| dw dv_2, \end{aligned} \quad (14)$$

where v'_1 and v'_2 are the outgoing velocities and $\mathbb{S}_-^{d-1}, \mathbb{S}_+^{d-1}$ are defined as:

$$\begin{aligned} \mathbb{S}_+^{d-1} &:= \mathbb{S}_+^{d-1}(v_i - v_j) = \{w \in \mathbb{S}^{d-1} : w \cdot (v_i - v_j) > 0\}, \\ \mathbb{S}_-^{d-1} &:= \mathbb{S}_-^{d-1}(v_i - v_j) = \{w \in \mathbb{S}^{d-1} : w \cdot (v_i - v_j) < 0\}, \end{aligned} \quad (15)$$

which are the half-spheres of \mathbb{S}^{d-1} , where the normal vector w has the same direction as $v_i - v_j$ in \mathbb{S}_+^{d-1} , and opposite direction in \mathbb{S}_-^{d-1} . Observe that if we rewrite w as $-w$ in the second integral of (14), we can simplify it to one term

$$\begin{aligned} C_{1,2}f_N^{(2)} &= \int_{\mathbb{R}^d} \int_{\mathbb{S}_+^{d-1}} \left(f_N^{(2)}(t, x_1, v'_1, x_1 + \epsilon w, v'_2) \right. \\ &\quad \left. - f_N^{(2)}(t, x_1, v_1, x_1 - \epsilon w, v_2) \right) ((v_2 - v_1) \cdot w)_+ dw dv_2, \end{aligned}$$

where (x_1, v'_1) and (x_2, v'_2) are the post-collision positions and velocities. Notice that we have changed the notation from $|((v_1 - v_2) \cdot w)|$ to $((v_2 - v_1) \cdot w)_+$, as we have restricted the domain to \mathbb{S}_+^{d-1} . Observe that we have obtained an expression that depends on $f_N^{(2)}$. Note that (13) is the first equation of the BBGKY hierarchy for hard-spheres [16], and shows the dependence of $f_N^{(1)}$ on $f_N^{(2)}$. We could repeat this process and we would observe that the equation for $f_N^{(2)}$, (11), involves $f_N^{(3)}$, and so on, creating a chain of equations that links each marginal distribution to the next, ultimately ending with the full N -particle distribution $f_N^{(N)}$. Further information on BBGKY hierarchy is given in [16].

In order to write a closed equation for the evolution $f_N^{(1)}$, we must look at the right-hand side of equation (13). We observe that the collision term depends on $f_N^{(2)}$. To address this dependence, we rely on

the *molecular chaos hypothesis*, which considers that velocities of colliding particles are uncorrelated, and therefore are locally independent of each other. This allows us to compute the probability that two particles with given velocities will collide by considering each particle separately. This is, the two-particle distribution function factorizes into the product of one-particle distributions. Then, if we define $f = \lim_{N \rightarrow \infty} f_N^{(1)}$, the *molecular chaos assumption* allows us to write:

$$f(t, z_1, z_2) \approx f(t, z_1)f(t, z_2).$$

Applying these considerations to equation (13), one finds that f should satisfy the Boltzmann equation

$$\partial_t f + v \cdot \nabla_x f = \alpha Q(f, f), \quad (16)$$

where the collisional operator is given by

$$Q[f, f](v) := \int_{\mathbb{S}_+^{d-1} \times \mathbb{R}^d} [f(v')f(v'_1) - f(v)f(v_1)]((v - v_1) \cdot w)_+ dw dv_1, \quad (17)$$

and the post-collision velocities v'_1 and v' are defined as

$$v' = v + w \cdot (v_1 - v)w, \quad v'_1 = v_1 - w \cdot (v_1 - v)w.$$

Note that $f(v')$, $f(v'_1)$, $f(v)$ and $f(v_1)$ are short notations for the expressions that include the position coordinates.

Observe that it is a difficult task to prove the convergence of the first marginal distribution function to the solution of the Boltzmann equation as $N \rightarrow \infty$, and in general it remains unproven globally in time. However, for small times (of the order of $1/\alpha$), Lanford's Theorem 2.1 allows us to justify the assumptions made when using the Boltzmann-Grad limit.

Theorem 2.1. (Lanford's Theorem). Consider a system of N particles interacting as hard-spheres of diameter ϵ . Let $f_0 : \mathbb{T}^d \times \mathbb{R}^d \mapsto \mathbb{R}^+$ be a continuous probability density such that

$$f_0(x, v) e^{\frac{\beta}{2}|v|^2} \leq e^{-\mu},$$

for some $\beta > 0$, $\mu \in \mathbb{R}$. Assuming that these N hard-spheres are initially distributed according to f_0 and independent (molecular chaos), there exists a positive time depending only on β and μ ($T^* = T^*(\beta, \mu)$) such that, in the Boltzmann-Grad limit, the distribution function of the particles converges uniformly on $[0, \frac{T^*}{\alpha}] \times \mathbb{T}^d \times \mathbb{R}^d$ to the solution of the Boltzmann equation.

The proof of this theorem is out of the scope of this thesis. However, a proof can be seen in [28].

2.3 From the linear Boltzmann equation to the heat equation

The main objective of this section is to ensure the existence of global solutions when studying the limit $\alpha \rightarrow \infty$, that is, when the collision frequency tends to infinity. To quantify the macroscopic dynamics over long times, we introduce a change of variables from the microscopic kinetic time, t , to a new macroscopic

time, τ .

Specifically, we define the time-scaling:

$$t = \alpha\tau. \quad (18)$$

It is necessary to remark that although the standard diffusive scaling involves scaling both space and time simultaneously, this is a particular case specific to the kinetic Boltzmann equation.

However, Boltzmann equation is not known to have global solutions for all times. So we will define a suitable setting in order to find them. In the nonlinear Boltzmann equation (16) that we have deduced, we linearize the collision operator by replacing $f(v'_1)$ and $f(v_1)$ by the stationary solution

$$M_\beta(v) := \left(\frac{\beta}{2\pi}\right)^{\frac{d}{2}} e^{-\frac{\beta}{2}|v|^2}, \quad \beta > 0.$$

Observe that $M_\beta(v)$ is the normalized Maxwellian distribution in a d -dimensional space, where $\beta = \frac{m}{k_B T}$ is the inverse temperature scaled by mass (where m is the particle mass, k_B is the Boltzmann constant, and T is the temperature). It appears as the equilibrium solution of the collision operator, that means that if collisions last enough time, the velocity distribution tends to M_β (i.e. equilibrium in velocities). It is used because the null space of \mathcal{Q} , the space of functions unchanged by collisions, is spanned by M_β .

Then, after replacing the collision particle distribution with the stationary solution $M_\beta(v)$, if we denote the distribution function of the incident particles by g_α , the equation becomes:

$$\partial_t g_\alpha + v \cdot \nabla_x g_\alpha = \alpha \iint [g_\alpha(v') M_\beta(v'_1) - g_\alpha(v) M_\beta(v_1)] ((v - v_1) \cdot \omega)_+ dv_1 d\omega. \quad (19)$$

We want to analyze the asymptotic behavior of $\tilde{g}_\alpha(\tau) := g_\alpha(\alpha\tau)$ in the limit $\alpha \rightarrow \infty$. To do so, we define, for our convenience,

$$\tilde{g}_\alpha(\tau, x, v) := M_\beta(v) \tilde{g}_\alpha(\tau, x, v). \quad (20)$$

Namely, it absorbs the Maxwellian weight into the distribution, simplifying and linearizing the collision operator.

Then, we proceed by applying the time-scaling defined in (18) to (19). Multiplying (19) by α , we obtain the scaled equation:

$$\partial_t \tilde{g}_\alpha + \alpha v \cdot \nabla_x \tilde{g}_\alpha = \alpha^2 \iint [\tilde{g}_\alpha(v') M_\beta(v'_1) - \tilde{g}_\alpha(v) M_\beta(v_1)] ((v - v_1) \cdot \omega)_+ dv_1 d\omega.$$

Now, considering that (20) implies $\tilde{g}_\alpha = M_\beta^{-1}(v) \tilde{\phi}_\alpha$, we can write:

$$\begin{aligned} M_\beta^{-1}(v) \partial_\tau \tilde{\phi}_\alpha + \alpha v \cdot \nabla_x (M_\beta^{-1}(v) \tilde{\phi}_\alpha) &= \\ \alpha^2 \iint [M_\beta^{-1}(v') \tilde{\phi}_\alpha(v') M_\beta(v'_1) - M_\beta^{-1}(v) \tilde{\phi}_\alpha(v) M_\beta(v_1)] ((v - v_1) \cdot \omega)_+ dv_1 d\omega. \end{aligned}$$

Note that as $M_\beta(v)$ does not depend on x or τ , we can multiply in both sides of the equation by $M_\beta(v)$ in order to isolate the left side of the expression

$$\begin{aligned} \partial_\tau \tilde{\phi}_\alpha + \alpha v \cdot \nabla_x (\tilde{\phi}_\alpha) &= \\ \alpha^2 \iint [M_\beta^{-1}(v') \tilde{\phi}_\alpha(v') M_\beta(v) M_\beta(v'_1) - \tilde{\phi}_\alpha(v) M_\beta(v_1)] ((v - v_1) \cdot \omega)_+ dv_1 d\omega. \end{aligned}$$

The next step is to simplify the first term of the integral. We use the principle of detailed balance, which asserts that at thermodynamic equilibrium, every elementary collision process is balanced by its exact reverse [32]. Physically, this arises because the underlying laws of motion are time-reversible (micro-reversibility) [26]. In our case, this principle ensures that $M_\beta(v)M_\beta(v_1) = M_\beta(v')M_\beta(v'_1)$. Notice that this equality holds because of conservation of energy $|v|^2 + |v_1|^2 = |v'|^2 + |v'_1|^2$. After applying this equality, the integral term simplifies to:

$$\alpha^2 \iint [\tilde{\phi}_\alpha(v')M_\beta(v_1) - \tilde{\phi}_\alpha(v)M_\beta(v_1)]((v - v_1) \cdot \omega)_+ dv_1 d\omega.$$

Grouping terms, we deduce that $\tilde{\phi}_\alpha(\tau, x, v)$ satisfies,

$$\partial_\tau \tilde{\phi}_\alpha + \alpha v \cdot \nabla_x \tilde{\phi}_\alpha = -\alpha^2 \iint [\tilde{\phi}_\alpha(v) - \tilde{\phi}_\alpha(v')]M_\beta(v_1)((v - v_1) \cdot \omega)_+ dv_1 d\omega.$$

This can be rewritten as

$$\begin{aligned} \frac{\partial \tilde{\phi}_\alpha}{\partial \tau} + \alpha v \cdot \nabla_x \tilde{\phi}_\alpha &= -\alpha^2 \mathcal{L} \tilde{\phi}_\alpha, \\ \mathcal{L} \tilde{\phi}_\alpha(v) &:= \iint [\tilde{\phi}_\alpha(v) - \tilde{\phi}_\alpha(v')]M_\beta(v_1)((v - v_1) \cdot \omega)_+ dv_1 d\omega, \end{aligned} \quad (21)$$

where \mathcal{L} is the linear form of \mathcal{Q} .

Now, we assume that we can write $\tilde{\phi}_\alpha(\tau, x, v)$ as an asymptotic expansion [15]

$$\tilde{\phi}_\alpha(\tau, x, v) = \tilde{\rho}_0(\tau, x, v) + \frac{1}{\alpha} \tilde{\rho}_1(\tau, x, v) + \frac{1}{\alpha^2} \tilde{\rho}_2(\tau, x, v) + \dots, \quad (22)$$

Then, we substitute this expansion into equation (21). We now regroup all terms from both sides of the equation by their corresponding power of α .

- $\mathcal{O}(\alpha^2)$ terms:

$$0 = -\alpha^2 \mathcal{L} \tilde{\rho}_0 \implies \mathcal{L} \tilde{\rho}_0 = 0$$

This is the highest-order term and only appears on the collision term.

- $\mathcal{O}(\alpha^1)$ terms: We write the terms of order α from both sides.

$$\alpha v \cdot \nabla_x \tilde{\rho}_0 = -\alpha \mathcal{L} \tilde{\rho}_1 \implies v \cdot \nabla_x \tilde{\rho}_0 + \mathcal{L} \tilde{\rho}_1 = 0$$

- $\mathcal{O}(\alpha^0)$ terms: Finally, we write the constant terms.

$$\partial_\tau \tilde{\rho}_0 + v \cdot \nabla_x \tilde{\rho}_1 = -\mathcal{L} \tilde{\rho}_2 \implies \partial_\tau \tilde{\rho}_0 + v \cdot \nabla_x \tilde{\rho}_1 + \mathcal{L} \tilde{\rho}_2 = 0$$

This development provides us the following set of equations:

$$\begin{aligned} \mathcal{L} \tilde{\rho}_0 &= 0, \\ v \cdot \nabla_x \tilde{\rho}_0 + \mathcal{L} \tilde{\rho}_1 &= 0, \\ \partial_\tau \tilde{\rho}_0 + v \cdot \nabla_x \tilde{\rho}_1 + \mathcal{L} \tilde{\rho}_2 &= 0. \end{aligned} \quad (23)$$

Observe that to find the solutions $\tilde{\rho}_0$, $\tilde{\rho}_1$ and $\tilde{\rho}_2$, one needs to be able to invert the operator \mathcal{L} . From the first equation in (23), one deduces that the operator \mathcal{L} acts only on the velocity variable v and that $\text{Ker}(\mathcal{L}) = \{\tilde{\rho}_0 : \mathcal{L}\tilde{\rho}_0 = 0\}$. Then, we conclude that $\tilde{\rho}_0$ is independent of the velocity.

Next, from the second equation of (23), since \mathcal{L} is invertible on the orthogonal complement of its kernel, we can formally invert it to deduce $\tilde{\rho}_1$. Defining $b(v) := \mathcal{L}^{-1}(v)$, we obtain that $\tilde{\rho}_1$ can be written as

$$\tilde{\rho}_1(\tau, x, v) = -b(v) \cdot \nabla_x \tilde{\rho}_0(\tau, x) + \bar{\rho}_1(\tau, x), \quad \bar{\rho}_1 \in \text{Ker } \mathcal{L}, \quad (24)$$

where $\bar{\rho}_1(\tau, x)$ is the homogenous solution. However, since $\bar{\rho}_1$ is also independent of the velocity v , the $\frac{1}{\alpha} \bar{\rho}_1$ term in the full expansion (22) can be absorbed into the $\tilde{\rho}_0$ term by a simple redefinition. Therefore, to ensure a unique decomposition, we set $\bar{\rho}_1 = 0$ without loss of generality.

Finally, from the third equation in (23), it can be shown that the existence of $\tilde{\rho}_2$ is guaranteed if $\partial_\tau \tilde{\rho}_0 + v \cdot \nabla_x \tilde{\rho}_1$ is orthogonal to the kernel of \mathcal{L}^* , the adjoint of \mathcal{L} . As \mathcal{L} is self-adjoint with respect to $M_\beta(v)$, then, the kernel of \mathcal{L} is the same as the one from \mathcal{L}^* . Thus, it can be deduced that it is necessary

$$\int_{\mathbb{R}^d} M_\beta(v) [\partial_\tau \tilde{\rho}_0 + v \cdot \nabla_x \tilde{\rho}_1] dv = 0. \quad (25)$$

Since $\tilde{\rho}_0$ is independent from v , this means that

$$\partial_\tau \tilde{\rho}_0 + \int_{\mathbb{R}^d} v \cdot \nabla_x \tilde{\rho}_1(\tau, x, v) M_\beta(v) dv = 0.$$

Now, we substitute the expression for $\tilde{\rho}_1$ given by (24) in (25)

$$\partial_\tau \tilde{\rho}_0 + \int_{\mathbb{R}^d} v \cdot \nabla_x (-b(v) \cdot \nabla_x \tilde{\rho}_0) M_\beta(v) dv = 0. \quad (26)$$

Since $b(v)$ is independent of x , we can extract it from the divergence operator. Also, recognizing that the term involves the divergence of the gradient, which corresponds to the Laplacian operator, we can rewrite (26) as

$$\begin{aligned} & \partial_\tau \tilde{\rho}_0 - \int_{\mathbb{R}^d} (v \cdot b(v)) [\nabla_x \cdot (\nabla_x \tilde{\rho}_0)] M_\beta(v) dv = 0 \\ & \implies \partial_\tau \tilde{\rho}_0 - \left(\int_{\mathbb{R}^d} v \cdot b(v) M_\beta(v) dv \right) \Delta_x \tilde{\rho}_0 = 0. \end{aligned} \quad (27)$$

Note that the integral term in the brackets represents the sum of diffusive contributions across all d spatial dimensions. However, due to the rotational symmetry of the Maxwellian M_β , the gas behaves identically in all directions. This physical symmetry ensures that the diffusion is uniform, meaning the total integral is simply the sum of d identical directional contributions. Therefore, to obtain the correct scalar diffusion coefficient κ_β (which applies to a single spatial direction), we must average this integral over the dimension d :

$$\kappa_\beta = \frac{1}{d} \int_{\mathbb{R}^d} v \cdot b(v) M_\beta(v) dv. \quad (28)$$

Substituting (28) back into (27), we obtain the final heat equation:

$$\partial_\tau \tilde{\rho}_0 - \kappa_\beta \Delta_x \tilde{\rho}_0 = 0. \quad (29)$$

Then, it can be deduced that the heat equation is the limit of the linear Boltzmann equation when using the scaling (18) and $\alpha \rightarrow \infty$. Some formality proves the following result.

Theorem 2.2. (*From linear Boltzmann equation to the heat equation*). Let ρ^0 be a bounded function, and let ρ denote the unique bounded solution to the heat equation

$$\partial_\tau \rho - \kappa_\beta \Delta_x \rho = 0 \quad \text{in } \mathbb{T}^d \times \mathbb{R}^d, \quad \rho|_{\tau=0} = \rho^0.$$

Let g_α be the unique solution to (19) with the initial condition

$$g_\alpha|_{t=0} = M_\beta \rho^0.$$

Then, for all $T > 0$, there exists a constant $C_T > 0$ such that

$$\sup_{\tau \in [0, T]} \sup_{(x, v) \in \mathbb{T}^d \times \mathbb{R}^d} |g_\alpha(\alpha \tau, x, v) - \rho(\tau, x) M_\beta(v)| \leq C_T \alpha^{-1/2}.$$

3. Kinetic equations for opinion dynamics

In this section, we are going to model the formation and spreading of opinions resulting from the interactions between agents within a society. To achieve this, we apply concepts from statistical mechanics, particularly the Boltzmann kinetic approach originally developed for gas dynamics and presented in Section 2.

We will first introduce a basic model to illustrate the fundamental ideas, and then present a more complete model that complements the previous approach by introducing more parameters and functions to capture social dynamics better.

However, before starting it is necessary to explain the difference between the interactions considered in opinions dynamics and the hard-sphere collisions derived in the previous section. In Section 2, the microscopic dynamics were governed by elastic collisions which conserved kinetic momentum and energy (see (2) and (3)). For opinions, interactions are governed by behavioral rules (such as compromise or diffusion) which generally do not conserve the “energy” (opinion variance) and the “momentum” (average opinion). Despite this difference in microscopic rules, the kinetic formalism remains valid, allowing us to derive a Boltzmann-type equation for the evolution of the opinion distribution.

3.1 “Classical” opinion dynamics Boltzmann equation

Let us consider a population of agents interacting in a society. To describe the microscopic state of the system, we associate to each agent a time-dependent random variable V_t , representing their opinion or social state at time t , which takes values in a bounded domain $\mathcal{V} = [-1, 1]$; where the states ± 1 indicate extreme opinions, while 0 represents indecisiveness or a neutral opinion. The random variable V_t is distributed according to a probability density $f(t, v)$ such for any subset $A \subset \mathcal{V}$:

$$P(V_t \in A) = \int_A f(t, v) dv.$$

Interactions between agents are modeled as “collisions” governed by an update rule, analogous to (5). Then, we can define the interaction between two individuals with pre-interaction opinions $V_t, V_t^* \in \mathcal{V}$ as follows:

$$\begin{aligned} V'_t &= V_t + I(V_t, V_t^*), \\ V_t^{*\prime} &= V_t^* + I_*(V_t^*, V_t), \end{aligned} \tag{30}$$

where V'_t and $V_t^{*\prime}$ denote the post-interaction opinions. Here, I and I_* are two different interaction functions defined in $\mathcal{V} \times \mathcal{V}$. In general, they are not equal, but if $I = I_*$, the interaction is said to be *symmetric*. Observe that in Section 2, the velocity $v \in \mathbb{R}^d$ had no boundaries. However, in our social model, the choice of I, I_* must ensure that the domain boundaries are respected; namely, we must guarantee that $V'_t, V_t^{*\prime} \in \mathcal{V}$ for all $V_t, V_t^* \in \mathcal{V}$.

Now, our objective is to obtain a Boltzmann-type equation for the opinion distribution similar to the one defined in (16). Then, for a given $\Delta t > 0$, two random agents with opinions V_t and V_t^* may meet and interact. If they do not interact, their opinions remain equal, however, if they do so, they update their social states as in (30). Note that, in real-world situations interactions are discrete events that occur

randomly over time. To describe this mathematically, we need to model the frequency of interaction. For this reason, and to account for the stochastic nature of social encounters, we introduce a Bernoulli random variable to determine if two individuals interact or not. Recall that a Bernoulli random variable is a discrete variable that takes the value 1 with probability p and 0 with probability $1 - p$. Specifically, the probability of an interaction occurring in a small time interval must be proportional to the length of that interval. If this probability was constant (independent of Δt), the interaction rate would diverge to infinity as $\Delta t \rightarrow 0$.

Therefore, we define the random variable T with a parameter proportional to Δt , specifically $T \sim \text{Be}(p = B\Delta t)$, where the probabilities are defined as

$$P(T = 1) = B\Delta t, \quad P(T = 0) = 1 - B\Delta t.$$

Here, the parameter $B > 0$ is the *interaction kernel*. Note that it is necessary that $B\Delta t \leq 1$ for $B\Delta t$ to be a probability.

Keeping these properties in mind, we can proceed to write the random interaction dynamics:

$$V_{t+\Delta t} = (1 - T)V_t + TV'_t, \tag{31}$$

$$V_{t+\Delta t}^* = (1 - T)V_t^* + TV_t^{*'}, \tag{32}$$

which can be rewritten in the form (30) as $V'_t := V_t + I(V_t, V_t^*)$ and $V_t^{*'} := V_t^* + I_*(V_t^*, V_t)$. The expressions (31) and (32) indicate that, after a time Δt , the opinions may or may not have changed, depending on whether an interaction took place.

Once we have defined the interactions, now we move to derive the evolution equation for the distribution $f(t, v)$. Let us consider any quantity ϕ that can be expressed as a function of an individual's opinion, i.e., $\phi = \phi(v)$. This function represents any observable property that can be computed from the opinion variable v . In our context, the function $\phi(v)$ may correspond to different measurable aspects of the opinion dynamics. For instance, it can represent the opinion itself, $\phi(v) = v$; its square, $\phi(v) = v^2$, which is often used to quantify opinion polarization; or the deviation from the mean opinion, $\phi(v) = |v - \bar{v}|$, which measures the distance of an individual's social state from the social average. Other choices could be $\phi(v) = e^{-\alpha|v - v_0|}$, which can describe the level of agreement or satisfaction relative to a particular opinion v_0 . Note that each choice of ϕ distinguish a different macroscopic aspect of the opinion distribution and provides new insights into the collective dynamics.

We are interested in the time evolution of the expected value of this observable quantity $\phi(v)$, denoted by $\langle \phi(V_t) \rangle$. Here, the bracket notation $\langle \cdot \rangle$ denotes the expected value (or mean value) of the random variable with respect to the density f . From (31), the value of the observable after a time interval Δt is:

$$\phi(V_{t+\Delta t}) = \phi((1 - T)V_t + TV'_t), \tag{33}$$

which can be understood, after a time Δt , as the value of ϕ may or may not have changed depending on whether an interaction occurred during that period.

The next step is to compute the average (or expected value) of both sides of (33) with respect to all the random variables involved. Since T is a Bernoulli random variable independent of the current state, we

can compute the expectation with respect to T by distinguishing the cases where an interaction occurs, $T = 1$, and where it does not, $T = 0$. Then, we have:

$$\begin{aligned}\langle \phi(V_{t+\Delta t}) \rangle &= \langle \phi((1-T)V_t + TV'_t) \rangle \\ &= (1-B\Delta t)\langle \phi(V_t) \rangle + B\Delta t\langle \phi(V'_t) \rangle,\end{aligned}$$

where we have computed explicitly the expectation with respect to T on the right side. Now, rearranging the terms and dividing by Δt , we get

$$\frac{\langle \phi(V_{t+\Delta t}) \rangle - \langle \phi(V_t) \rangle}{\Delta t} = \langle B(\phi(V'_t) - \phi(V_t)) \rangle. \quad (34)$$

Observe that in the limit $\Delta t \rightarrow 0^+$, the left-hand side of (34) becomes the time derivative of the expected value $\langle \phi(V_t) \rangle$, yielding the following expression

$$\frac{d}{dt}\langle \phi(V_t) \rangle = \langle B(\phi(V'_t) - \phi(V_t)) \rangle. \quad (35)$$

Similarly, for (32) we have

$$\frac{d}{dt}\langle \phi(V_t^*) \rangle = \langle B(\phi(V_t^{*'}) - \phi(V_t^*)) \rangle, \quad (36)$$

and after adding expressions (35) and (36) we obtain

$$\frac{d}{dt}\langle \phi(V_t) + \phi(V_t^{*'}) \rangle = \langle B(\phi(V'_t) - \phi(V_t) + \phi(V_t^{*'}) - \phi(V_t^*)) \rangle. \quad (37)$$

Notice that we have added (35) and (36) because the particles are indistinguishable and, as a consequence, the total variation is the sum of both contributions.

After this process, we are now capable of deducing an equation for the distribution function f . We assume that both V_t and $V_{*,t}$ are distributed according to $f(t, v)$, this is:

$$\langle \phi(V_t) \rangle = \langle \phi(V_t^*) \rangle = \int_{\mathcal{V}} \phi(v) f(t, v) dv.$$

On the other hand, we can write

$$\begin{aligned}&\left\langle B \left(\phi(V'_t) - \phi(V_t) + \phi(V_t^{*'}) - \phi(V_t^*) \right) \right\rangle \\ &= \int_{\mathcal{V}} \int_{\mathcal{V}} B \left(\phi(v') - \phi(v) + \phi(v') - \phi(v_*) \right) f(t, v) f(t, v_*) dv dv_*.\end{aligned} \quad (38)$$

In equation (38), by applying the update rule for opinions (30), the post-interaction opinions v' and v_*' are determined by the pre-interaction opinions v and v_* . Also, the *molecular chaos assumption* has been used to write $f(t, v, v_*) = f(t, v)f(t, v_*)$. Developing (37) and taking into account the previous expressions, we get

$$\begin{aligned}\frac{d}{dt}\langle \phi(V_t) \rangle &= \frac{d}{dt} \int_{\mathcal{V}} \phi(v) f(t, v) dv \\ &= \int_{\mathcal{V}} \int_{\mathcal{V}} \frac{1}{2} B \left(\phi(v') - \phi(v) + \phi(v') - \phi(v_*) \right) f(t, v) f(t, v_*) dv dv_*,\end{aligned} \quad (39)$$

This equation is the *weak form* for f , as it has to hold for any choice of ϕ .

However, rearranging and making a suitable change of variables we can obtain the *strong form*. First, we

will rewrite the right-hand side separating into the *gain* terms (the ones containing $\phi(v')$ and $\phi(v'_*)$) and the *loss* terms (those containing $-\phi(v)$ and $-\phi(v_*)$):

$$\begin{aligned} \frac{d}{dt} \int_{\mathcal{V}} \phi(v) f(t, v) dv &= \frac{1}{2} \int_{\mathcal{V}} \int_{\mathcal{V}} B(\phi(v') + \phi(v'_*)) f(v) f(v_*) dv dv_* \\ &\quad - \frac{1}{2} \int_{\mathcal{V}} \int_{\mathcal{V}} B(\phi(v) + \phi(v_*)) f(v) f(v_*) dv dv_*. \end{aligned} \tag{40}$$

Observe that we can rewrite the loss expression because the integral is symmetric in (v, v_*) and, as a consequence, we have the simplified form:

$$\frac{1}{2} \int_{\mathcal{V}} \int_{\mathcal{V}} B(\phi(v) + \phi(v_*)) f(v) f(v_*) dv dv_* = \int_{\mathcal{V}} \int_{\mathcal{V}} B\phi(v) f(v) f(v_*) dv dv_*.$$

Now, we will focus on the gain term

$$\frac{1}{2} \int_{\mathcal{V}} \int_{\mathcal{V}} B(\phi(v') + \phi(v'_*)) f(v) f(v_*) dv dv_*.$$

We treat the two identical terms $\phi(v')$ and $\phi(v'_*)$ separately. We consider the term with $\phi(v')$:

$$I := \frac{1}{2} \int_{\mathcal{V}} \int_{\mathcal{V}} B(v, v_*) \phi(v') f(v) f(v_*) dv dv_*.$$

Assuming that the map $(v, v_*) \mapsto (v', v'_*) = T(v, v_*)$ is invertible, and denoting with

$$J = \left| \det \frac{\partial(v', v'_*)}{\partial(v, v_*)} \right|$$

the absolute value of the Jacobian determinant from pre-collisional opinions (v, v_*) to post-collisional opinions (v', v'_*) , we can apply the change of variables in I . Note that, under this change,

1. $dv dv_* = \frac{1}{J} dv' dv'_*$
2. $I = \frac{1}{2} \int_{\mathcal{V}} \int_{\mathcal{V}} \frac{1}{J} B(T^{-1}(v', v'_*)) \phi(v) f(T_1^{-1}(v', v'_*)) f(T_2^{-1}(v', v'_*)) dv' dv'_*,$

where T_1 and T_2 indicates the first and second components of the map T , respectively. Observe that v', v'_* are just integration variables, so we can rename them as $v' \mapsto v$ and $v'_* \mapsto v_*$, and the expression becomes:

$$I = \frac{1}{2} \int_{\mathcal{V}} \int_{\mathcal{V}} \frac{1}{J} B(T^{-1}(v, v_*)) \phi(v) f(T_1^{-1}(v, v_*)) f(T_2^{-1}(v, v_*)) dv dv_*. \tag{41}$$

After defining $(\tilde{v}, \tilde{v}_*) := T^{-1}(v, v_*)$, (41) can be read as

$$I = \frac{1}{2} \int_{\mathcal{V}} \int_{\mathcal{V}} \frac{1}{J} B(\tilde{v}, \tilde{v}_*) \phi(v) f(v) f(\tilde{v}) f(\tilde{v}_*) dv dv_*. \tag{42}$$

A similar procedure applies to the term involving $\phi(v'_*)$. By symmetry of the interaction, we find that this term yields an identical contribution to the term involving $\phi(v')$ given in (42). Consequently, the total gain term corresponds to two times the integral (42). Now, plugging the gain and loss terms into (40), we get

$$\frac{d}{dt} \int \phi(v) f(t, v) dv = \int_{\mathcal{V}} \int_{\mathcal{V}} \left\{ \frac{1}{J} B(\tilde{v}, \tilde{v}_*) f(\tilde{v}) f(\tilde{v}_*) - B(v, v_*) f(v) f(v_*) \right\} \phi(v) dv dv_*. \tag{43}$$

Then, as ϕ is an arbitrary test function, one can determine that the collision operator $\mathcal{Q}(f, f)(v)$ may be identified with the integrand in braces in (43). Hence, we obtain the *strong form*:

$$\partial_t f(t, v) = \int_{\mathcal{V}} \left(\frac{1}{J} B(\tilde{v}, \tilde{v}_*) f(\tilde{v}) f(\tilde{v}_*) - B(v, v_*) f(v) f(v_*) \right) dv_*,$$

where $(\tilde{v}, \tilde{v}_*) = T^{-1}(v, v_*)$ are the pre-interaction opinions that result in the post-interaction state (v, v_*) . Relabelling the variables, one can write:

$$\partial_t f(t, v') = \int_{\mathcal{V}} \left(\frac{1}{J} B(v, v_*) f(v) f(v_*) - B(v', v'_*) f(v') f(v'_*) \right) dv'_*, \quad (44)$$

where v and v_* have to be considered as functions of v' and v'_* .

3.2 Compromise and diffusion in opinions

In this Section, we extend the previous framework to a more realistic scenario where agents not only exchange opinions but are also subject to random diffusion (representing noise or uncertainty in the communication) and explicitly account for individual compromise.

As in Section 3.1, the opinion v is a scalar variable in the bounded domain $\mathcal{V} = [-1, 1]$. Moreover, we assume that interactions preserve the bounds. Thus, we model the collisions with a new update rule, as we did in (30). We define the interaction between two agents' opinions $v, v_* \in \mathcal{V}$ as:

$$\begin{aligned} v' &= v - \gamma P(|v|)(v - v_*) + \eta D(|v|), \\ v'_* &= v_* - \gamma P(|v_*|)(v_* - v) + \eta_* D(|v_*|), \end{aligned} \quad (45)$$

where (v, v_*) are the pre-interaction opinions and (v', v'_*) are the post-interaction social states.

Note that this model is more complex than the one presented before, as it introduces more parameters and functions to characterize the social dynamics. First, we introduce the constant parameter $\gamma \in (0, 1/2)$, which represents the compromise propensity. This parameter quantifies how strongly agents adjust their opinions during an interaction. The upper bound ($\gamma < 1/2$) ensures that post-interaction opinions remain in the range of pre-interaction ones (in the absence of noise).

Secondly, to model the random uncertainty in human interactions such as the influence of random external factors or sudden agents deviations, we introduce two random variables η and η_* . These variables have zero mean and variance σ^2 , and take values in a bounded set (support) $\mathcal{B} \subseteq \mathbb{R}$. Note that σ models the modification of opinion due to diffusion (or noise), representing the degree of unpredictability in the opinion exchange.

Finally, the functions $P(\cdot)$ and $D(\cdot)$ modulate the local relevance of compromise and diffusion for a given opinion, respectively. We assume that $P(|v|)$ and $D(|v|)$ are defined between $[0, 1]$ and are non-increasing with respect to $|v|$. This implies that agents with extreme opinions ($|v| \approx 1$) are less likely to compromise. Conversely, the behavior of D near the boundaries is designed to ensure that the diffusion term does not push opinions out of the interval $[-1, 1]$.

As in Section 3.1, we consider $f(t, v)$ as the distribution of an opinion $v \in \mathcal{V}$ at time $t \geq 0$. To derive the

evolution equation for $f(t, v)$, we follow the same kinetic approach detailed in Section 3.1. Specifically, we proceed by computing the evolution of the expected value of observable quantities $\phi(v)$ as introduced in (33). Taking the limit $\Delta t \rightarrow 0$ leads to the weak formulation analogous to (39). Finally, by separating gain and loss terms and applying the change of variables described in (40), we recover the *strong form* (44) for $f(t, v)$. Notice that the Jacobian J ensures the preservation of mass for any choice of the interaction kernel (or transition rate) B . In this model, we define it as follows:

$$B_{(v, v_*) \rightarrow (v', v'_*)} = \Theta(\eta)\Theta(\eta_*)\chi(|v'| \leq 1)\chi(|v'_*| \leq 1), \quad (46)$$

where $\Theta(\cdot)$ is a symmetric probability density with zero mean and variance σ^2 , representing the distribution of the noise. The term $\chi(\cdot)$ denotes the indicator function, defined such that $\chi(A) = 1$ if the condition A is true, and $\chi(A) = 0$ otherwise. We include these indicator functions to explicitly enforce the domain boundaries; they ensure that any interaction which would result in an opinion outside the interval $[-1, 1]$ has zero probability of happening, thus preserving the physical bounds of the model. The interaction kernel defines the probability density for an interaction between two individuals with opinions (v, v_*) to produce post-interaction opinions (v', v'_*) . It characterizes the frequency of interactions and random variability through Θ and Θ_* , taking into account that bounds cannot be violated.

Furthermore, to prevent diffusion noise from generating a drastic change of opinion, it is considered that, in principle, the support \mathcal{B} of the symmetric random variables, defined at the start of this section, is a subset of \mathcal{V} . Observe that for a general Θ , the transition rate B depends on the opinion variables (v, v_*) through the indicator variables χ . However, if we select parameters and functions properly and, consequently, guarantee that $|v'|, |v'_*| \leq 1$, one can deduce that the kernel B no longer depends on the social states [23]. Further explanation is given in Subsection 4.3.3.

4. Monte Carlo methods for kinetic equations

In this section, we introduce a numerical method used to simulate the kinetic models described in previous chapters. As established in Section 2 and Section 3, the Boltzmann kinetic equation describes the evolution of a probability distribution function $f(t, x, v)$ in a high-dimensional phase space.

Standard deterministic numerical methods, such as finite difference, finite volume, finite elements or spectral methods [24], face a significant obstacle that is the high dimensionality of the phase space. For instance, to discretize a $2d$ -dimensional phase space with M grid points per dimension, one needs M^{2d} total points. Thus, for a standard 3-dimensional problem ($d = 3$), this results in M^6 points, which causes a high computational cost in order to integrate with precision [23]. Furthermore, the collision operator $\mathcal{Q}(f, f)$ involves a multi-dimensional non-linear integral that needs to be evaluated at every point in space and time.

To overcome these complications, we employ probabilistic techniques known as Monte Carlo methods.

4.1 Preliminaries

The Monte Carlo method encompasses a broad class of computational algorithms that rely on repeated random sampling to obtain numerical results. The fundamental principle is based on the Law of Large Numbers, which states that, by simulating a large number of independent random events, the empirical average of the results converges to the theoretical expected value [6]. This method is mainly used when calculating an exact solution with a deterministic algorithm is unfeasible due to computational cost or impossible to calculate an exact solution with a deterministic algorithm [25]. Typical applications include computing difficult integrals, complex systems with many degrees of freedom and simulating social or economic systems [18].

The modern formalism of Monte Carlo methods date back to the 1940s at the Los Alamos National Laboratory. The concept was conceived by Stanislaw Ulam in 1946 while playing solitaire during his recovery from an illness. He realized that determining the probability of winning a hand was mathematically intractable using pure combinatorics but could be easily approximated by simulating many random hands and counting the successes. He shared this awareness with John Von Neumann, and together they developed the method on the ENIAC (Electronic Numerical Integrator And Computer), the first electronic computer, initially created to solve the neutron diffusion problems encountered in the Manhattan Project. The term “Monte Carlo” was proposed by Nicholas Metropolis, a reference to the Monte Carlo Casino in Monaco, symbolizing the element of randomness inherent in the method [20, 19].

In the specific context of kinetic theory, the main development occurred in the 1960s with the creation of the Direct Simulation Monte Carlo (DSMC) method by Graeme Bird. Originally developed for aerospace to simulate rarefied gas dynamics, Bird’s method was a breakthrough in the way of solving the Boltzmann equation, because it simulated the gas itself instead of trying to compute the mathematical expression [3, 4]. Despite initially being considered a phenomenological model, it was later rigorously proved by Wolfgang Wagner (1992) that the DSMC process converges to the solution of the Boltzmann equation [31].

A remarkable feature of Monte Carlo methods is their convergence rate. The error in approximating an integral via Monte Carlo scales as $\mathcal{O}(N^{-1/2})$, where N is the number of samples. Essentially, this rate is

independent of the dimension d of the integration space. In contrast, standard deterministic grid methods (such as Simpson's rule or finite differences) typically have an error scaling of $\mathcal{O}(N^{-r/d})$, where r depends on the order of the scheme. As the dimension d increases, the convergence rate of deterministic methods decreases rapidly. For high-dimensional problems like the Boltzmann equation ($d = 6$ for a 3D gas), the dimension-independent convergence of Monte Carlo makes it the best computational choice [6].

4.2 Fundamental features and assumptions of DSMC

The DSMC method is distinct from standard numerical integration techniques. Instead of attempting to discretize the integro-differential Boltzmann on a grid (as we would do in finite differences), DSMC simulates the time evolution of the physical system itself. However, it is computationally impossible to simulate the exact trajectory of every single particle for macroscopic systems.

For this reason, DSMC is based on a set of fundamental physical assumptions that allow us to simulate the system's behavior using a probabilistic approach. These assumptions are founded in the scale separation inherent to dilute systems, where the average distance between particles is much larger than the particle diameter ϵ . Consequently, the duration of an interaction is negligible compared to the time between interactions.

Decoupling of motion and interaction. The first and main assumption is that the trajectory motion and the interactions can be decoupled over a sufficiently small time interval Δt .

In a real physical system, particles move and collide simultaneously. However, in a dilute gas (or a large society), which is characterized by a low particle density where the volume occupied by the particles themselves is negligible compared to the total volume of the container, the duration of a collision event can be neglected when comparing it to the time a particle spends moving freely between collisions (the mean free time) [22, 5]. This allows us to split the continuous time evolution of the system into two steps:

- **Free Transport:** All particles move in straight lines according to their velocity vectors without interacting.
- **Interaction:** Some particles “stop” moving for a small time interval and undergo collisions or opinion exchanges.

This justifies the time-splitting technique that we will detail in Subsection (4.3.1). For this assumption to hold, the time step Δt must be chosen small enough as compared to the mean collision time τ , i.e. $\Delta t < \tau$.

Stochasticity of interactions. The second assumption is that the impact parameters and initial velocities of colliding pairs are inherently random. In a deterministic molecular dynamics simulation, one only would need to compute the exact trajectory of each particle to determine if they hit. In DSMC, we change this approach to a stochastic one: we select collision pairs and post-collision velocities probabilistically from the distributions predicted by the Boltzmann collision integral.

The simulation particle and statistical weight. The third assumption is related to the magnitude of the system. A real macroscopic gas contains on the order of 10^{23} molecules; a country may have 10^7

voters. Simulating this exact number of agents is unfeasible.

DSMC assumes that is not necessary to simulate the exact number of real particles (N_{real}) in order to obtain an accurate description of the distribution function. Instead, we simulate a smaller number of particles (N_{sim}). Each simulated particle represents a large number W of real, like-minded individuals. This ratio is known as *statistical weight*

$$W = \frac{N_{real}}{N_{sim}}.$$

This allows us to approximate the continuous distribution function $f(t, v)$ using a finite sample size, with the accuracy of the approximation governed by the Law of Large Numbers.

4.3 Mathematical tools for DSMC

Having established the physical assumptions that justify the Direct Simulation approach, we now introduce the specific mathematical tools required to implement them numerically: the splitting algorithm for the time evolution of the inhomogeneous equation, random generating techniques for generating stochastic events and generalization of the collision kernel. For the implementation of DSMC, we will consider the three dimensional space \mathbb{R}^3 .

4.3.1 The splitting approach

The Boltzmann equation (16) describes the evolution of $f(t, x, v)$, which is a non-negative function describing the time evolution of the distribution of particles moving with velocity $v \in \mathbb{R}^3$ at position $x \in \Omega \subset \mathbb{R}^3$ at time $t > 0$, due to two physical processes: free transport and interactions. Numerical integration of this integro-differential equation is complex because the transport term involves spatial derivatives, while the collision term is local in space but non-local in velocity. To solve this problem, the most common approach is based on a time-splitting. In the context of numerical analysis and fluid dynamics limits, it is a standard convention to express the Boltzmann equation in terms of the *Knudsen number*, a dimensionless parameter proportional to the mean free path between collisions. To align with the standard literature and our computational implementation, we define the Knudsen number as

$$\varepsilon := \frac{1}{\alpha},$$

where α is the inverse of the mean free path, introduced in Section 2.2. Using this notation, we can rewrite (16) as:

$$\frac{\partial f}{\partial t} + v \cdot \nabla_x f = \frac{1}{\varepsilon} Q(f, f).$$

Notice that a small value of ε ($\varepsilon \ll 1$) implies a high collision frequency (fluid regime), and as a consequence, we should use Navier-Stokes equation. However, for $\varepsilon \gg 1$, we are in a free molecular flow. For $\varepsilon \approx 1$, we are in a rarefied regime and the appropriate model to use would be the Boltzmann equation.

Now, we consider the following initial value problem:

$$\begin{cases} \frac{\partial f}{\partial t} + v \cdot \nabla_x f = \frac{1}{\varepsilon} Q(f, f), \\ f(0, x, v) = f_0(x, v). \end{cases} \quad (47)$$

Then, the solution after one time step Δt may be split into two steps. First, we solve the space homogeneous equation (collision step) for all $x \in \Omega$ for a time step Δt ,

$$\begin{cases} \frac{\partial \tilde{f}}{\partial t} = \frac{1}{\varepsilon} Q(\tilde{f}, \tilde{f}), \\ \tilde{f}(0, x, v) = f_0(x, v). \end{cases} \quad (48)$$

Note that this step updates the velocities (or opinions) based on interactions. The parameter ε now controls the “stiffness” of the collision term: a small ε (high collision frequency) implies that the system approaches local equilibrium described by the Euler or Navier-Stokes equations.

Finally, we integrate the transport equation (convection step), where we use the solution of the previous step as initial condition,

$$\begin{cases} \frac{\partial f}{\partial t} + v \cdot \nabla_x f = 0, \\ f(0, x, v) = \tilde{f}(\Delta t, x, v). \end{cases} \quad (49)$$

4.3.2 Random sampling techniques

Since DSMC is inherently stochastic, the algorithm frequently requires generating random numbers distributed according to specific probability density functions, denoted by $p(x)$. We have several ways to do this task, however, we mention only two of them, which are the ones that we have employed.

- **Standard Computational Libraries:** For standard probability distributions - such as Gaussian or Exponential - we use high-performance scientific libraries (e.g. Python’s *Numpy* or *Scipy*). These provide highly optimized generators that ensure both computational efficiency and numerical stability.
- **The Acceptance-Rejection Method:** For complex or non-standard distributions (such as specific interaction kernels or initial distribution of velocities/opinions) where the cumulative distribution function cannot be easily inverted, we use the Acceptance-Rejection method, proposed by Von Neumann in 1951 [30]. This technique generates samples from a target density $p(x)$ by filtering samples from a simpler proposal density $w(x)$ similar to the original one.

4.3.3 The collision kernel

To implement the collision step (48), we must explicitly define the collision kernel appearing in the operator $Q(f, f)$. In classical kinetic theory for gas dynamics, the kernel B characterizes the details of binary interactions and generalizes the specific hard-sphere term derived in Section 2.

In the general case of the Boltzmann equation (16), the collision operator is written as:

$$Q(f, f)(v) = \int_{\mathbb{R}^d} \int_{\mathbb{S}^{d-1}} B(|v - v_*|, \omega) [f(v')f(v'_*) - f(v)f(v_*)] d\omega dv_*,$$

where the kernel B typically takes the form of a Variable Hard Sphere (VHS) model:

$$B(|v - v_*|, \omega) = C_\lambda |v - v_*|^\lambda.$$

This kernel characterizes the physics of interactions and encompasses several physical models:

- For hard spheres ($\lambda = 1$), as in (16), the collision rate grows proportionally to relative velocity, meaning that faster particles collide with more frequency. This corresponds to the term $((v - v_1) \cdot \omega)_+$ derived in Section 2.
- For Maxwellian molecules ($\lambda = 0$), the kernel is constant ($B = C$). This simplifies the numerical algorithm considerably as the collision rate remains uniform.

For opinion dynamics, the interaction kernel is determined by the frequency of social exchanges.

- For simpler models, as in Section 3.1, we assumed a constant interaction rate B . This is equivalent to the Maxwellian case, where every pair of agents have the same probability of interacting.
- For more complex models, as in Section 3.2, the interaction kernel might depend on the opinion distance ($|v - v_*|$) or other factors.

4.4 Direct simulation schemes

In the previous section we explained a time-splitting technique to decouple the Boltzmann equation into a transport step and a collision step. While the transport step is exact and deterministic (particles move in straight lines), the collision step requires solving the spatially homogeneous Boltzmann equation (48). Solving this equation deterministically is complex and computationally expensive due to the high-dimensional nature of the collisional operator \mathcal{Q} . To overcome this, we employ DSMC schemes; which evolve the particle system stochastically, interpreting the collisional operator as a probabilistic jump process in the velocity (or opinion) space. In this subsection, we present some of these DSMC schemes.

To motivate the numerical formulation, we first return to the structure of the collision operator (17) using the general kernel B defined in Subsection 4.3.3. This operator describes the net rate of change of the distribution function f due to binary collisions and can be decomposed into two distinct terms: a gain term \mathcal{Q}^+ and a loss term \mathcal{Q}^- , resulting in the splitting:

$$\mathcal{Q}(f, f) = \mathcal{Q}^+(f, f) - \mathcal{Q}^-(f, f).$$

The gain term $\mathcal{Q}^+(f, f)$ describes the increase of the density $f(v)$ due to particles scattering into the velocity state v . This occurs when particles with velocities v' and v'_* interact to produce a particle with velocity v . Consequently, this term depends on the distribution of the post-collisional velocities $f(v')f(v'_*)$.

The loss term $\mathcal{Q}^-(f, f)$ describes the decay of the density $f(v)$ due to particles leaving the state v . This corresponds to the direct collision process, where a particle with velocity v interacts with another particle v_* and scatters into new velocities. This term depends on the distribution of the pre-collisional velocities $f(v)f(v_*)$. The expressions for these terms are obtained by directly splitting the collision integral:

$$\mathcal{Q}(f, f)(v) = \underbrace{\int_{\mathbb{R}^d} \int_{\mathbb{S}_+^{d-1}} B(|v - v_*|, \omega) f(v') f(v'_*) d\omega dv_*}_{\mathcal{Q}^+(f, f)} - \underbrace{\int_{\mathbb{R}^d} \int_{\mathbb{S}_+^{d-1}} B(|v - v_*|, \omega) f(v) f(v_*) d\omega dv_*}_{\mathcal{Q}^-(f, f)}.$$

In the loss term \mathcal{Q}^- , we observe that the distribution $f(v)$ is independent of the integration variables v_* and ω . This allows us to factorize it:

$$\mathcal{Q}^-(f, f)(v) = f(v) \left(\int_{\mathbb{R}^d} \int_{\mathbb{S}_+^{d-1}} B(|v - v_*|, \omega) f(v_*) d\omega dv_* \right).$$

The integral in the brackets represents the total rate at which a particle with velocity v suffers collisions. For the construction of the numerical scheme, we assume that this rate is bounded. We define a constant μ that serves as an upper bound for this integral.

Then, we can rewrite (48) in the form:

$$\frac{\partial f}{\partial t} = \frac{1}{\varepsilon} [P(f, f) - \mu f] = \frac{1}{\varepsilon} (\mathcal{Q}^+ - \mathcal{Q}^-), \quad (50)$$

where $\mu \neq 0$ is a constant and $P(f, f)$ is a non-negative bilinear operator such that

$$\frac{1}{\mu} \int_{\mathbb{R}} P(f, f)(v) \phi(v) dv = \int_{\mathbb{R}} f(v) \phi(v) dv, \quad \phi(v) = 1, v, v^2.$$

In particular, for the case of Maxwellian molecules, we have $P(f, f) = \mathcal{Q}^+(f, f)$, where $\mathcal{Q}^+(f, f)$ is the gain term of the collision operator; and also have that $\mu f = \mathcal{Q}^-(f, f)$, where $\mathcal{Q}^-(f, f)$ is the loss term.

4.4.1 Nanbu-Babovsky's scheme

We consider a time interval $[0, t_{max}]$, discretized in n_{TOT} intervals of size Δt . Also, let us denote $f^n(v)$ an approximation of $f(v, n\Delta t)$. The scheme is based on a probabilistic interpretation of the Forward Euler time discretization proposed by Nanbu (1980). Using the collision form derived in (50), the solution is updated as

$$\frac{f^{n+1} - f^n}{\Delta t} = \frac{1}{\varepsilon} \mathcal{Q}(f^n, f^n) = \frac{1}{\varepsilon} [P(f^n, f^n) - \mu f^n].$$

Rearranging the terms to solve for f^{n+1} , we obtain:

$$f^{n+1} = f^n + \frac{\Delta t}{\varepsilon} P(f^n, f^n) - \frac{\mu \Delta t}{\varepsilon} f^n.$$

By grouping the terms proportional to f^n and multiplying by μ in the $P(f^n, f^n)$ term, we can rewrite the update rule as

$$f^{n+1} = \left(1 - \frac{\mu \Delta t}{\varepsilon}\right) f^n + \frac{\mu \Delta t}{\varepsilon} \frac{P(f^n, f^n)}{\mu}. \quad (51)$$

One can deduce that if f^n is a probability density, then, both $P(f^n, f^n)/\mu$ and f^{n+1} are probability densities. Thus, we can deduce a probabilistic interpretation from this equation. In the physical sense, a particle with velocity v_i will not collide with probability $(1 - \mu \Delta t / \varepsilon)$, and it will collide with probability $\mu \Delta t / \varepsilon$, according to the collision law described by $P(f^n, f^n)/\mu$. In the Monte Carlo level, to sample v_i from f^{n+1} , with probability $(1 - \mu \Delta t / \varepsilon)$ we sample from f^n and with probability $\mu \Delta t / \varepsilon$ we sample from $P(f^n, f^n)/\mu$. Observe that it is necessary that $\Delta t \leq \varepsilon/\mu$ to have the probabilistic interpretation.

We start by considering kinetic equations for Maxwellian molecules such as (50), in which $P(f, f) = \mathcal{Q}^+(f, f)$ and $B = C$. In 1980, Nanbu proposed an algorithm [21] based on the probabilistic interpretation (51):

Algorithm 1 Nanbu for a Maxwellian Gas

```

1: Sample initial particle velocities  $\{v_i^0, i = 1, \dots, N\} \sim f_0(\mathbf{v})$ 
2: for  $n = 0$  to  $n_{TOT} - 1$  do
3:   for  $i = 1$  to  $N$  do
4:     draw a uniform random number  $\xi \sim U(0, 1)$ 
5:     if  $\xi < 1 - \mu\Delta t/\varepsilon$  then
6:       no collision:  $v_i^{n+1} = v_i^n$ 
7:     else
8:       select random index  $j \in \{1, \dots, N\} \setminus \{i\}$ 
9:       compute  $v'_j$  by performing the collision between particle  $i$  and  $j$ 
10:      update:  $v_i^{n+1} = v'_j$ 
11:    end if
12:  end for
13: end for

```

Note that for this algorithm we do not have a control on the numbers of collisions that are being simulated, due to the random number ξ . Despite the theoretical convergence of Algorithm 1 to the solution of the Boltzmann equation as $N \rightarrow \infty$, this scheme has a significant drawback for finite systems: it does not conserve momentum and energy at the microscopic level. This is because for each particle i , its velocity when colliding with a particle j is updated based on the rules (4) while the velocity of particle j remains unchanged. To solve this, Babovsky introduced a conservative version [2] in which independent particle pairs are selected, and both of their velocities are updated at each collision.

This new version has a computational advantage as it eliminates the inner loop for the particles. We achieve this by selecting the number of pairs that are going to collide. In order to do it, we calculate the expected value of particles colliding in a small time step Δt , which is obtained by multiplying the number of simulated particles N by the probability of collision $\mu\Delta t/\varepsilon$. As a consequence, the number of expected collisions is $\mu\Delta t/2\varepsilon$. Having stated this change, we present the following algorithm:

Algorithm 2 Nanbu-Babovsky (NB) for a Maxwellian Gas

```

Sample initial particle velocities  $\{v_i^0, i = 1, \dots, N\} \sim f_0(\mathbf{v})$ 
for  $n = 0$  to  $n_{TOT} - 1$  do
  set  $N_c = \text{Round}(N\mu\Delta t/2\varepsilon)$ 
  select  $N_c$  pairs  $(i, j)$  uniformly among all possible pairs and:
    compute the collision between  $i$  and  $j$ , then compute  $v'_i, v'_j$ 
    set  $v_i^{n+1} = v'_i, v_j^{n+1} = v'_j$ 
    set  $v_k^{n+1} = v_k^n$  for the particles that have not been selected
end for

```

In this algorithm, the function $\text{Round}(x)$ denotes a stochastic rounding function, with $x \in \mathbb{R}^n$. In [23] is chosen

$$\text{Round}(x) = \begin{cases} \lceil x \rceil + 1 & \text{with probability } x - \lceil x \rceil \\ \lceil x \rceil & \text{with probability } 1 - (x - \lceil x \rceil) \end{cases}$$

where $\lceil x \rceil$ denotes the integer part of x .

5. Numerical Experiment

To validate the Nanbu-Babovsky Algorithm 2, we test it against the Kac equation, a simplified dimensional model of the Boltzmann equation. We use this model for validation because there is an exact analytical solution, and therefore we can compute errors between the theoretical solution and the one obtained from the simulation. This serves as a way to validate the numerical method before applying it to the study of opinion dynamics. All the codes and results from Sections 5 and 6 can be found in the following *GitHub* repository: <https://github.com/brunofernandez-blip/TFG.git>.

5.1 The Kac equation

The Kac equation describes the evolution of the distribution function $f(t, v)$ for $v \in \mathbb{R}$, and can be written as

$$\frac{\partial f}{\partial t} = \frac{1}{\varepsilon} \int_0^{2\pi} \int_{-\infty}^{+\infty} \frac{1}{2\pi} [f(v')f(v'_*) - f(v)f(v_*)] dv_* d\theta. \quad (52)$$

The collision operator acts as a rotation in the velocity plane of two interacting particles. In particular, if two particles with velocities v, v_* collide, their post-collision velocities are updated by:

$$v' = v \cos \theta - v_* \sin \theta, \quad v'_* = v \sin \theta + v_* \cos \theta.$$

where θ is a scattering angle chosen uniformly from $[0, 2\pi]$, or as stated in [23], $\theta = 2\pi Rand$, where $Rand \sim U(0, 1)$. Notice that the Kac equation is of the form (50) with

$$P(f, f) = \frac{1}{2\pi} \int_0^{2\pi} \int_{-\infty}^{+\infty} f(v')f(v'_*) dv_* d\theta,$$

and $\mu = \int_{-\infty}^{\infty} f(v)dv$.

The analytical solution of the equation (52) is deduced in [17], and is given by:

$$f(t, v) = \frac{1}{2} \left[\frac{3}{2}(1 - C(t))\sqrt{C(t)} + (3C(t) - 1)C(t)^{3/2}v^2 \right] e^{-C(t)v^2}, \quad (53)$$

where $C(t) = \left[3 - 2e^{-\sqrt{\pi}t/16} \right]^{-1}$.

Since the DSMC method evolves a finite set of N discrete particles, the simulation returns a list of velocities $\{v_j(t)\}_{j=1}^N$ at any given discrete time t . To compare these numerical results with the continuous analytical solution $f(t, v)$ defined in (53) and compute error norms, we must reconstruct a smooth probability density function from the particle data.

We achieve this by using a mollification technique. We first introduce a uniform velocity grid indexed by an integer I , denoted as $\{V_I\}_{I=0}^{N_g}$, covering the domain of interest $\{V_I = V_{\min} + I\Delta V, I = 0, \dots, N_g\}$. We then define the reconstructed numerical solution $f_{num}(t, v)$ as the convolution of the empirical particle distribution with a smoothing kernel (or mollifier) W_H , as done in [10]:

$$f_{num}(t, v) = \frac{1}{N} \sum_{j=1}^N W_H(v - v_j(t)). \quad (54)$$

For the numerical computation of error norms, (54) is evaluated at the specific grid points $v = V_I$.

For the smoothing kernel W_H , we employ a B-spline form with bandwidth H :

$$W_H(x) = \frac{1}{H} W\left(\frac{x}{H}\right), \quad W(x) = \begin{cases} 3/4 - |x|^2 & \text{if } |x| \leq 0.5, \\ (|x| - 3/2)^2/2 & \text{if } 0.5 < |x| \leq 1.5, \\ 0 & \text{otherwise.} \end{cases}$$

The parameter H controls the resolution of the reconstruction. We select $H = 0.2$ and $\Delta V = 0.0625$ as a compromise: a smaller H would resolve finer details but introduce statistical noise (fluctuations), while a larger H would smooth out features and introduce bias.

5.1.1 Normalization of the analytical solution

In order to validate the numerical results we must ensure the consistency of the analytical benchmark. The exact solution to the Kac equation, given in (53), is not normalized (it does not integrate to 1), so we must account for this before comparing it to the numerical results.

Let us consider the general form of the analytical solution provided in (53). To determine if this function represents a valid probability density function, we compute its integral over the velocity space $v \in \mathbb{R}$. To do so, we use the standard Gaussian integrals:

$$\int_{-\infty}^{+\infty} e^{-av^2} dv = \sqrt{\frac{\pi}{a}}, \quad \int_{-\infty}^{+\infty} v^2 e^{-av^2} dv = \frac{1}{2a} \sqrt{\frac{\pi}{a}}.$$

Renaming $a = C(t)$, the integral $I(t) = \int_{-\infty}^{+\infty} f(t, v) dv$ becomes:

$$I(t) = \frac{1}{2} \left[\frac{3}{2}(1 - C(t))\sqrt{C(t)} \left(\sqrt{\frac{\pi}{C(t)}} \right) + (3C(t) - 1)C(t)^{3/2} \left(\frac{\sqrt{\pi}}{2C(t)^{3/2}} \right) \right].$$

Simplifying the terms inside the brackets:

$$\begin{aligned} I(t) &= \frac{1}{2} \left[\frac{3\sqrt{\pi}}{2}(1 - C(t)) + \frac{\sqrt{\pi}}{2}(3C(t) - 1) \right] \\ &= \frac{\sqrt{\pi}}{4} (3 - 3C(t) + 3C(t) - 1) = \frac{2\sqrt{\pi}}{4} \\ &= \frac{\sqrt{\pi}}{2}. \end{aligned}$$

Consequently, the integral of the analytical solution is constant in time but distinct from unity:

$$I(t) = \frac{\sqrt{\pi}}{2} \approx 0.8862, \quad \forall t \geq 0.$$

The Nanbu-Babovsky scheme is conservative by construction. As a consequence, the reconstructed numerical distribution $f_{num}(t, v)$ defines a valid probability density function over the velocity space, satisfying the normalization condition:

$$\int_{-\infty}^{+\infty} f_{num}(t, v) dv = 1.$$

Since the analytical solution yields a total probability mass of $I(t) \approx 0.8862$ (instead of 1), a direct comparison between the raw values would be misleading. To address this, we introduce a normalization constant K :

$$K = \frac{1}{I(t)} = \frac{2}{\sqrt{\pi}} \approx 1.1284.$$

In the results presented in Section 5.2, the numerical distribution is scaled by a factor of $1/K$. This adjustment allows us to make a direct comparison between the numerical results and the exact analytical solution.

5.1.2 Asymptotics of the solution of the Kac equation

A fundamental property of kinetic equations is the relaxation to thermodynamic equilibrium. To validate that our simulation captures this physical behavior, we study the asymptotic limit $t \rightarrow \infty$ of the exact solution (53).

First, recall the definition of the time-dependent scaling function $C(t)$ given in (53). Note that as $t \rightarrow \infty$, the exponential term decays to zero. Consequently, the scaling factor converges to a constant:

$$C_\infty = \lim_{t \rightarrow \infty} C(t) = \lim_{t \rightarrow \infty} \frac{1}{3 - 2e^{-\frac{\sqrt{\pi}}{16}t}} = \frac{1}{3 - 0} = \frac{1}{3}.$$

Now, in order to obtain $f_\infty(v)$, we replace back the value $C_\infty = \frac{1}{3}$ into (53):

$$\begin{aligned} f_\infty(v) &= \lim_{t \rightarrow \infty} f(t, v) = \frac{1}{2} \left[\frac{3}{2}(1 - C_\infty)\sqrt{C_\infty} + (3C_\infty - 1)C_\infty^{3/2}v^2 \right] e^{-C_\infty v^2} \\ &= \frac{1}{2} \left[\frac{1}{\sqrt{3}} \right] e^{-\frac{1}{3}v^2} = \frac{1}{2\sqrt{3}} e^{-\frac{v^2}{3}}. \end{aligned}$$

Then, we can write

$$f_\infty(v) = \frac{1}{2\sqrt{3}} e^{-\frac{v^2}{3}}. \quad (55)$$

Note that the resultant function $f_\infty(v)$ has the form of a Gaussian distribution centered in zero with variance $\sigma^2 = \frac{3}{2}$. Furthermore, as shown in Subsection 5.1.1, this asymptotic function, (55), maintains the same probability mass $I_\infty = \frac{\sqrt{\pi}}{2}$, needing the same normalization factor K .

5.2 Numerical results

In this section, we try to reproduce the results presented [23] to validate our implementation. All of these simulations were performed using $N = 5 \times 10^4$ particles and setting the parameters $H = 0.2$, $\Delta V = 0.0625$, as stated in Subsection 5.1. Also, we set $\mu = \int_{-\infty}^{\infty} f(t, v) dv = \frac{\sqrt{\pi}}{2}$, $\forall t \geq 0$.

We first examine the ability of the Nanbu-Scheme to capture the non-equilibrium features of the Kac equation solution. To achieve this, Figure (3) presents the solution obtained with the simulation at $t = 2$ with time step $\Delta t = 1.0$ (represented by orange crosses), compared with the exact analytical solution (blue line).

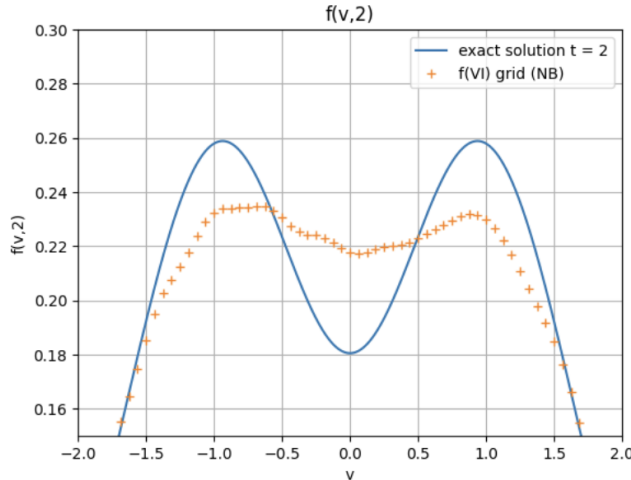


Figure 3: Reconstructed probability density function at $t = 2.0$ for $\Delta t = 1.0$ obtained from our Nanbu-Babovsky simulation (orange crosses) compared to the exact analytical solution (53) (blue line). $N = 5 \times 10^4$ particles.

As shown in Figure 3, we are able to reproduce the results presented in [23] with high fidelity. The location of the peaks ($v = \pm 0.9$) and the depth of the central valley are captured accurately. The minor fluctuations observed in our plot may be attributed to the stochastic noise inherent in the Monte Carlo method, but the overall bimodal structure is captured with high fidelity.

5.2.1 Quantitative comparison.

Having established the qualitative agreement between the simulation and the reference benchmark, we now quantify the accuracy of our implementation. To do this, we computed the L^2 error between the reconstructed numerical solution f_{num} given by (54), and the exact analytical solution f given in (53).

The error at a given time t is computed using numerical integration, and can be written as:

$$E_{L^2}(t) = \left(\int_{v_{min}}^{v_{max}} |f_{num}(t, v) - f(t, v)|^2 dv \right)^{1/2}. \quad (56)$$

In our implementation, this integral is approximated using Simpson's rule over the discretized velocity grid defined in Subsection 5.1. Specifically, we defined the velocity bounds as $v_{min} = V_{min} = -5$ and $v_{max} = V_{max} = 5$. Consequently, the number of grid intervals N_g of size ΔV is determined by:

$$N_g = \frac{V_{max} - V_{min}}{\Delta V} = \frac{10.0}{0.0625} = 160.$$

Thus, the simulation domain is defined as $V \in [-5.0, 5.0]$ with $N_g + 1 = 161$ discrete grid points. After discretizing our integration domain, we proceed to analyze the temporal evolution of the error.

To analyze the convergence properties of the scheme, we computed the time evolution of the L^2 error between the reconstructed numerical solution and the analytical solution over the interval $t \in [0, 6]$. We performed two simulations with different time steps, $\Delta t = 0.5$ and $\Delta t = 0.2$, while keeping the number of

particles fixed at $N = 5 \times 10^4$. The results are compared in Figure 4.

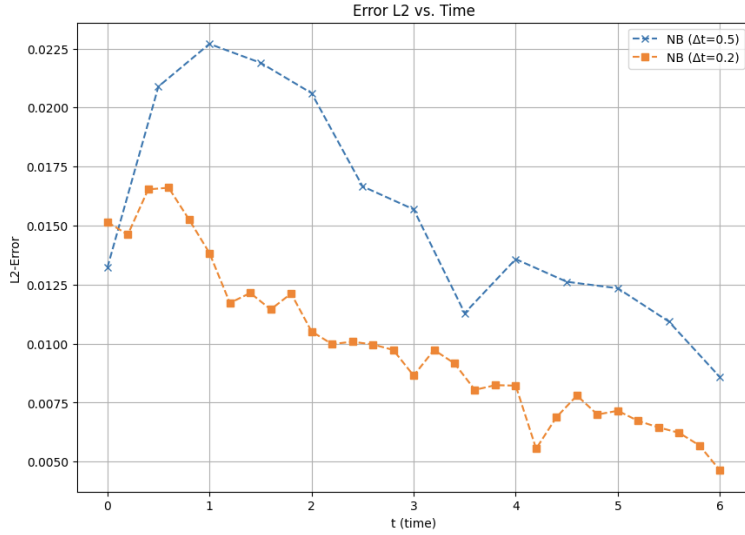


Figure 4: Time evolution of the L^2 error norm (56) between the numerical and exact solutions for the Nanbu-Babovsky simulation with time steps $\Delta t = 0.5$ (blue dashed line) and $\Delta t = 0.2$ (orange dashed line) for $t \in [0, 6]$.

A comparison of the two curves reveals that we are able to faithfully reproduce the results presented in [23]. Note that both simulations exhibit a characteristic behavior, the L^2 error rises initially to reach a maximum peak around $t \approx 1.0$, and subsequently decays monotonically as the system approaches equilibrium.

Notice that the simulation with $\Delta t = 0.2$ yields a consistently lower error compared to the $\Delta t = 0.5$ case. Specifically, the peak error decreases from approximately 0.023 to 0.016. Furthermore, this improved accuracy is maintained throughout the simulation; at $t = 6$, the error for the smaller time step drops to approximately 0.005, compared to nearly 0.009 for the larger case.

Despite the stochastic variance inherent in finite-particle Monte Carlo methods, the global trend, the magnitude of the error, and the rate of error decay are consistent with the standard benchmarks, confirming the numerical convergence of the scheme.

5.2.2 Influence of time discretization

To complete the numerical validation, a further study was conducted to determine the influence of the time discretization parameter, Δt , on the global accuracy of the Nanbu-Babovsky scheme. While Figure 4 showed convergence of the solution for specific cases, it is necessary to characterize the convergence behavior of the simulation as the time step approaches zero.

To achieve this, we performed a series of simulations over the time interval $t \in [0, 8]$, keeping the spatial discretization fixed ($V \in [-5, 5]$, $N_g = 160$) and the number of particles constant at $N = 5 \times 10^4$. The time step Δt was varied across two orders of magnitude to cover distinct regimes of temporal resolution: $\Delta t \in \{1.0, 0.5, 0.1, 0.05, 0.01\}$.

For each simulation configuration, the accuracy was quantified by computing the L^2 error norm between the numerical approximation and the exact solution at every time step as in (56). This error is calculated via numerical integration using Simpson's rule over the discretized velocity grid, as done in Subsection 5.2.1. This allows us to rigorously track the global deviation of the particle distribution throughout the entire simulation time. Figure (5) shows the temporal evolution of the L^2 error for the selected time steps.

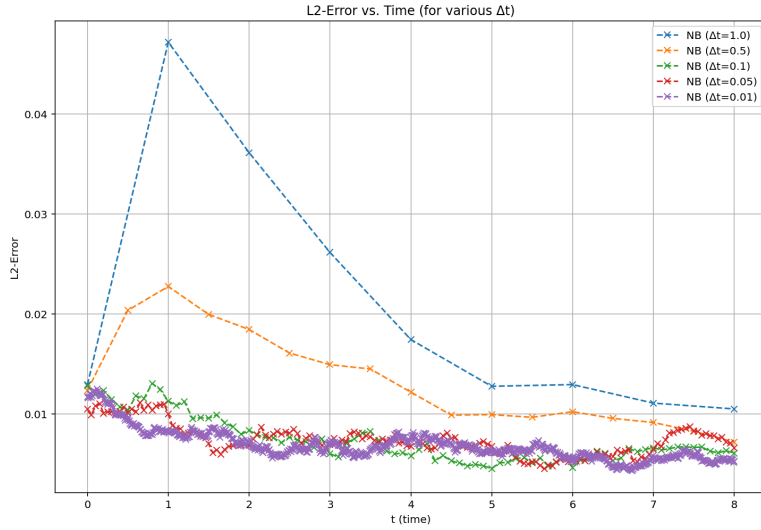


Figure 5: Temporal evolution of the L^2 error norm (56) between the numerical and exact solutions for varying time steps $\Delta t \in \{1.0, \dots, 0.01\}$. All simulations were performed with a fixed sample size of $N = 5 \times 10^4$ particles.

A clear convergence trend can be observed, as Δt is reduced from 1.0 to 0.01, the global error decreases significantly, particularly during the initial phase of the simulation. However, the behavior of the error varies distinctly depending on the time interval considered.

During the initial phase of the temporal evolution, specifically for $t \in [0, 4]$, the influence of the time step is most notable. In this interval, the analytical solution $f(t, v)$ undergoes rapid temporal changes as it relaxes towards its asymptotic state. The simulations with large time steps ($\Delta t = 1.0$ and 0.5) exhibit a large error peak around $t \approx 1.0$, indicating that they fail to capture the rapid relaxation dynamics of the system.

However, for $t > 4$, the solution $f(t, v)$ approaches the stationary state f_∞ , and consequently, its evolution in time slows down significantly. As observed in Figure 5, decreasing the time step Δt leads to a reduction in the error, confirming the convergence of the numerical scheme as $\Delta t \rightarrow 0$. Consequently, we can conclude that a small time step is critical for capturing the initial variations.

5.2.3 Sensitivity and scaling of the parameter ε

To further characterize the robustness of the Nanbu-Babovsky scheme, we examined the impact of the scaling parameter ε on the accuracy of the solution.

In order to do this, a key modification was required in our code compared to the one used for the previous analysis. Note that in Subsection 5.2.2, $\varepsilon = 1$ was a constant value, while we varied the number of time steps Δt . However, in this case, we will vary ε . Observe that as we approach the fluid regime ($\varepsilon \ll 1$), the collision term becomes stiff. A first idea to analyze this sensitivity would be fixing the time step Δt , nonetheless, for small values of ε , the collision probability ($P_{\text{coll}} \approx \mu \Delta t / \varepsilon$) deduced in Subsection 4.4.1 would exceed unity if Δt is not small enough, violating the conservation constraints of Nanbu-Babovsky scheme and causing the simulation to fail.

To prevent our simulation to fail our code was adapted. We imposed a linear constraint coupling the time step to the scaling parameter:

$$\Delta t = 0.2\varepsilon.$$

Note that this choice corresponds to a collision probability ($P_{\text{col}} \approx 0.2$), which is a safe margin selected to control the time discretization error while ensuring that the number of collisions N_c remains smaller than the total number of available particle pairs. Under this adaptive constraint, we performed simulations for a range of scaling parameters $\varepsilon \in \{1.0, \dots, 0.005\}$, which were performed for $t \in [0, 30]$.

To quantify the deviation of the simulations from the analytical solution for the different values of ε , we computed the L^2 error between the analytical solution given by (53) and the reconstructed numerical solution for each value. Figure (6) presents the evolution of this error as a function of ε for various snapshots (for $T = 2.0, 4.0, 6.0, 8.0, 10.0, 12.0, 14.0, 18.0, 22.0, 26.0, 30.00$).

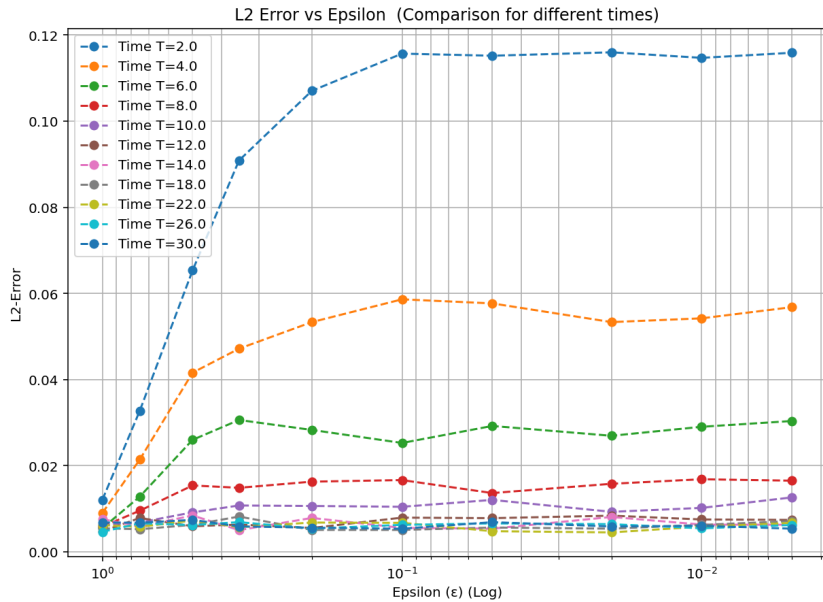


Figure 6: L^2 deviation from the analytical solution as a function of the scaling parameter ε . The time step was adapted as $\Delta t = 0.2\varepsilon$ to maintain stability.

The plot shows two distinct behaviors depending on the physical state of the system. First, during the early stages of the simulation, which encompasses time from $T = 2.0$ to approximately $T = 10.0$, we observe an increase in the L^2 error as $\varepsilon \rightarrow 0$. In particular, the error starts increasing as we decrease ε , and at a certain value of ε , the error remains stationary. This is a consequence of reducing ε , which

causes the system to accelerate its dynamics. In particular, for $T = 2.0$ (blue dashed line), the error increases significantly as we decrease ε . This behavior indicates that the numerical scheme faces challenges in resolving the stiff relaxation dynamics characteristic of the fluid limit ($\varepsilon \approx 0$). At these early times, the solution evolves extremely rapidly for small ε , leading to larger deviations from the exact analytical trajectory compared to the kinetic regime ($\varepsilon = 1$).

However, for longer times ($T \geq 12.0$), the error stabilizes to a minimum value (≈ 0.005) regardless of the parameter ε . This confirms that once the rapid initial relaxation is complete, the Nanbu-Babovsky scheme correctly captures the solution across all scaling regimes with high accuracy.

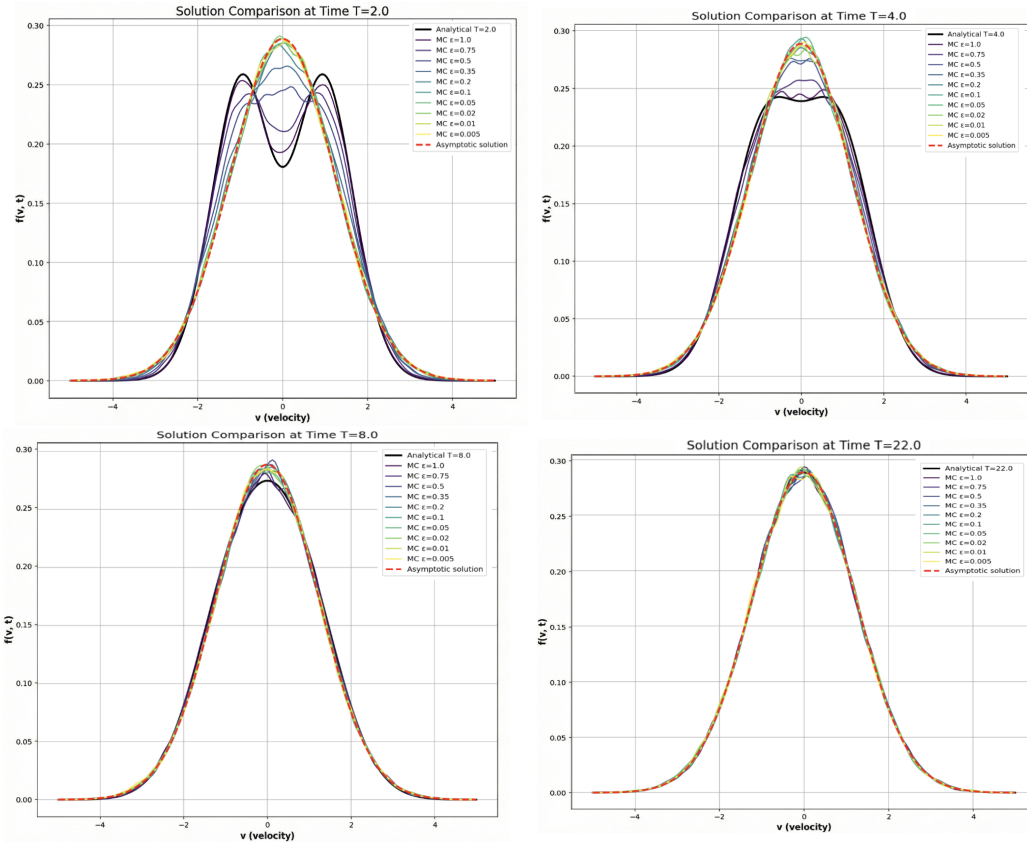


Figure 7: Temporal evolution of the particle distribution function $f(t, v)$ for various scaling parameters $\varepsilon \in [0.005, 1.0]$. The panels display the numerical solution at four distinct time snapshots: (top left) $T = 2.0$, (top right) $T = 4.0$, (bottom left) $T = 8.0$, and (bottom right) $T = 22.0$. In each subplot, the solid black line corresponds to the exact analytical solution, while the red dashed line represents the asymptotic Maxwellian solution (55). The colored curves represent the Monte Carlo simulation results, ranging from dark purple for the kinetic regime ($\varepsilon = 1.0$) to yellow for the fluid limit ($\varepsilon = 0.005$).

To visualize this acceleration effect, Figure 7 compares the reconstructed probability density functions of the particles for different values of the scaling parameter ε at four chosen instants ($T = 2.0, 4.0, 8.0, 22.0$). The four snapshots in Figure 7 provide a clear visualization of how the scaling parameters alter the relaxation dynamics. At the earliest stage ($t = 2.0$, Top Left), the distinction between the physical regimes is most pronounced. The simulation with $\varepsilon = 1.0$ follows with high fidelity the exact analytical solution, preserving the characteristic bimodal shape of the non-equilibrium distribution. In contrast, the simulations

in the fluid limit ($\varepsilon \leq 0.05$, yellow/green lines) have already collapsed to the asymptotic stationary solution f_∞ , which corresponds to the Maxwellian distribution defined in (55) (represented with the red dashed line). This behavior shows the physical role of the scaling parameter ε . A small value corresponds to a high collision frequency, resulting in many interactions per time step. This large number of collisions forces the system to relax towards the thermodynamic equilibrium f_∞ almost instantaneously.

As time progresses through $t = 4.0$ and $t = 8.0$, we observe the gradual relaxation of the kinetic regime. The bimodal structure of the $\varepsilon = 1.0$ case smoothens out as the peaks merge, slowly approaching the central Gaussian shape, while the fluid regime solutions remain stable at the equilibrium state. Finally, by $t = 22.0$ (bottom right), the system has reached a stationary state. At this stage, the differences between the scaling regimes vanish, and all simulations, regardless of their ε value, overlap almost perfectly with the analytical Maxwellian solution f_∞ .

The observed behavior demonstrates that the Nanbu-Babovsky scheme correctly captures the stiffness of the collision operator in the kinetic regime.

6. Numerical Analysis : Opinion Dynamics

Having validated the numerical stability and convergence of the Nanbu-Babovsky scheme using the Kac equation defined in Section 5, we now apply this method to the main objective of this project : the kinetic modeling of opinion formation.

While the Kac equation is an excellent example that provides an excellent framework for mathematical analysis, it describes a simplified physical interaction (collisions in a Maxwellian gas). In this section, we transition from physical particle systems to *Sociophysics*, solving the Boltzmann-type equations that model how agents in a society adjust their continuous opinions through binary interactions. The goal is to analyze how macroscopic behaviors, such as polarization, consensus or fragmentation, emerge from microscopic rules of compromise and diffusion.

6.1 The kinetic model and interaction rules

Adapting the kinetic framework introduced in Section 3.2, we consider a population of agents whose opinions are represented by a continuous variable $v \in \mathcal{V} = [-1, 1]$, where $v = \pm 1$ represent extreme opposite views. Following the kinetic framework established by Toscani [27] and Düring [12], we model the social dynamics through pairwise interactions.

We briefly recall the interaction rules defined in Section 3.2. Let two agents with pre-interaction opinions v and v_* meet. Their post-interaction opinions v' and v'_* are updated according to the following rules:

$$\begin{aligned} v' &= v - \gamma P(|v - v_*|)(v - v_*) + \eta D(|v|), \\ v'_* &= v_* - \gamma P(|v_* - v|)(v_* - v) + \eta_* D(|v_*|), \end{aligned} \quad (57)$$

where $\gamma \in (0, \frac{1}{2})$ is a parameter that quantifies how strongly agents adjust their opinions during an interaction, and η and η_* are independent random variables with zero mean and variance σ^2 , representing the stochastic noise or random uncertainty inherent in human interactions.

The opinion dynamics are governed by two key functions, P and D , which characterize the sociology of the interaction.

First, to model the phenomenon of bounded confidence, we define the compromise propensity P as an indicator function that depends on the relative distance between opinions of the two interacting agents:

$$P(|v - v_*|) = \mathbb{1}_{|v - v_*| \leq r} = \begin{cases} 1 & \text{if } |v - v_*| \leq r, \\ 0 & \text{if } |v - v_*| > r, \end{cases} \quad (58)$$

where r denotes the confidence radius or tolerance threshold. This definition implies that agents only interact if their opinions are sufficiently close; if the distance $|v - v_*$ is greater than r , the compromise term is not taken into account, and the agents effectively ignore each other, undergoing only diffusion.

Secondly, we introduce a variable diffusion coefficient $D = D(|v|)$ to model the stochastic noise or the relevance of self-thinking. To ensure that opinions remain bounded within the domain $\mathcal{V} = [-1, 1]$ and to

model the fact that extremal opinions are more difficult to change than moderate ones, we define:

$$D(|v|) = (1 - |v|^2)^\nu, \quad \nu \geq 0. \quad (59)$$

Note that this function implies that the diffusion vanishes at the boundaries $v = \pm 1$. Consequently, agents holding extreme opinions are modeled as being less susceptible to random fluctuations than moderate agents, reflecting a higher degree of conviction.

It is necessary to remark the distinction of this interaction rule from the one introduced theoretically in Section 3.2. In that model, the compromise function was defined as $P(|v|)$, depending only on the agent's individual state. That definition modeled dogmatism or stubbornness, meaning that an agent with an extreme opinion ($|v| \approx 1$) would simply refuse to compromise, regardless of who they interacted with.

In contrast, the model considered in (57) defines the compromise propensity as $P(|v - v_*|)$, depending on the relative distance between the opinions of the interacting agents. This captures the sociological phenomenon of bounded confidence, which occurs when an extremist might interact with another extremist of the same faction (since $|v - v_*|$ is small), but will ignore a moderate or an opposer (since $|v - v_*|$ is large). This transition from an individual ($P(|v|)$) to a pairwise ($P(|v - v_*|)$) dependency is crucial as it allows the model to capture the formation of isolated sub-groups and local clusters that we will analyze in the numerical results.

6.2 Numerical implementation

To solve the system dynamics derived in Section 6.1, we adapt the Nanbu-Babovsky scheme previously studied in Section 5.2. While the fundamentals of the algorithm remain consistent, relying on the stochastic simulation of particle pairs to approximate the collision integral, the specific interaction kernel requires a significant modification to incorporate the sociological mechanism of bounded confidence.

Unlike the Kac equation, where every selected pair undergoes a collision (represented as a rotation in velocity space), social interactions in this model are conditional. The simulation proceeds by discretizing time into steps of size Δt , as we did for the Kac equation. At each time step, the population of N agents is randomly partitioned into $\frac{N}{2}$ pairs. For every pair (i, j) , we first compute the opinion distance $d_{ij} = |v_i - v_j|$. The evolution of their opinions is then determined by comparing this distance against the confidence radius r introduced in (58). If the distance d_{ij} is less or equal to the threshold r , the interaction occurs. The agents influence each other, updating their opinions according to the compromise rule, while simultaneously experiencing the stochastic diffusion modeled by $D(v)$. Conversely, if the distance exceeds the radius ($d_{ij} > r$, the compromise term vanishes ($P = 0$)). In this case, the agents ignore each other socially but remain subject to the diffusion process, representing independent self-thinking or external noise.

A final numerical consideration related to the stochastic nature of the diffusion term should be taken into account. One can observe that the selection of the diffusion function $D(v)$ ensures that for each opinion $v \in [-1, 1]$, its image $D(v) = (1 - v^2)^\nu$, with $\nu \geq 0$, is inside the opinion domain $\mathcal{V} = [-1, 1]$. However, since the Gaussian noise η theoretically has infinite support, there exists a small probability, which cannot be neglected, that an update pushes an agent's opinion outside the domain $[-1, 1]$. To guarantee mathematical consistency and stability, we apply a projection operator at the end of each time step. This operator enforces the boundary conditions by projecting any value outside the opinion domain onto the

nearest boundary:

$$v_i^{new} = \text{proj}_{[-1,1]}(\tilde{v}_i) = \min(1, \max(-1, \tilde{v}_i)),$$

where \tilde{v}_i is the provisional opinion computed by the interaction rule.

Having established all these rules, we can now present the Nanbu-Babovsky applied to opinion dynamics:

Algorithm 3 Nanbu-Babovsky Scheme for Opinion Dynamics

```

1: Define  $N$  (number of agents),  $N_{TOT}$  (time steps),  $\Delta t$  (time step size)
2: Define  $\gamma$  (compromise),  $\sigma$  (noise std.),  $r$  (confidence radius),  $\nu$  (diffusion exponent)
3: Sample initial opinions  $v_i^0$  from  $f_0(v)$  for  $i = 1 \dots N$ 
4: for  $n = 0$  to  $N_{TOT} - 1$  do
5:   Select  $N/2$  pairs  $(i, j)$  uniformly among all agents without replacement
6:   for each selected pair  $(i, j)$  do
7:     Compute opinion distance  $d_{ij} = |v_i^n - v_j^n|$ 
8:     Generate independent noise  $\eta_1, \eta_2 \sim \mathcal{N}(0, \sigma^2)$ 
9:     if  $d_{ij} \leq r$  then
10:       $\tilde{v}_i = v_i^n - \gamma(v_i^n - v_j^n) + \eta_1(1 - (v_i^n)^2)^\nu$ 
11:       $\tilde{v}_j = v_j^n - \gamma(v_j^n - v_i^n) + \eta_2(1 - (v_j^n)^2)^\nu$ 
12:    else
13:       $\tilde{v}_i = v_i^n + \eta_1(1 - (v_i^n)^2)^\nu$ 
14:       $\tilde{v}_j = v_j^n + \eta_2(1 - (v_j^n)^2)^\nu$ 
15:    end if
16:     $v_i^{n+1} = \min(1, \max(-1, \tilde{v}_i))$ 
17:     $v_j^{n+1} = \min(1, \max(-1, \tilde{v}_j))$ 
18:  end for
19: end for
    
```

6.3 Numerical results

To characterize the macroscopic behavior of the system, we performed a series of numerical simulations using the Nanbu-Babovsky scheme described in Algorithm 3. Unless otherwise specified, the simulations were performed with a population of $N = 10^4$ agents, a compromise parameter $\gamma = 0.25$, and a fixed time step $\Delta t = 0.05$ to ensure stability. The diffusion exponent was set to $\nu = 2$, as done in [12] to ensure that the noise vanishes at the boundaries.

6.3.1 Influence of bounded confidence (r)

In the first experiment, we analyze the role of the confidence radius r , which models the tolerance of agents to opinions different from their own. We fixed a low noise level ($\sigma = 0.01$) to isolate the effects of the compromise function P . Then, we performed several simulations varying $r \in \{0.05, 0.2, 0.5, 1.0\}$. Regarding the initial conditions, we employed an uniform distribution over $[-1, 1]$, representing a society with maximally diverse opinions and no initial bias.

Figure 8 provides a comprehensive view of the system's dynamics for increasing values of r (arranged from top to bottom). The left column displays the final opinion histograms at the end of the simulation ($t = 25$). The right column visualizes the temporal evolution of the opinion trajectories for a representative subset of agents, showing how individual opinions drift and cluster over time.

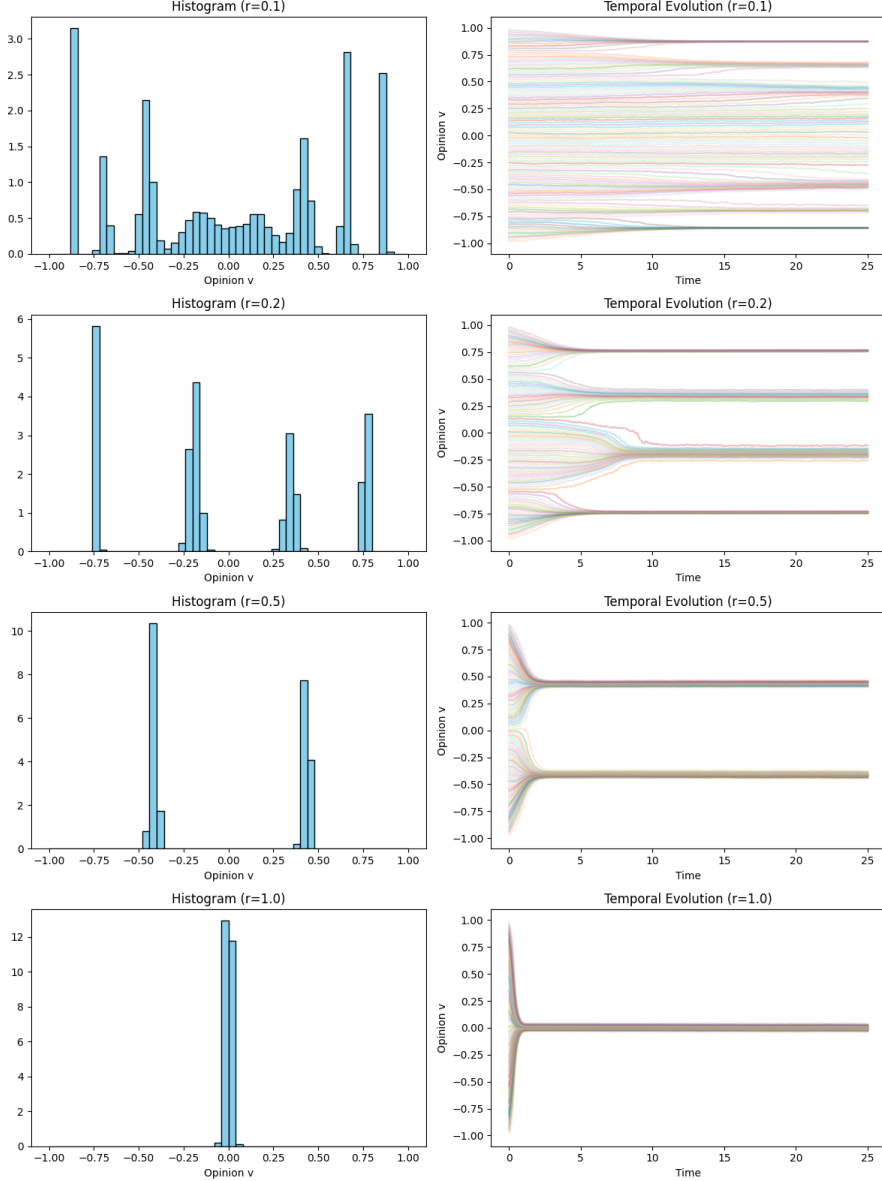


Figure 8: Influence of the bounded confidence radius r on the macroscopic opinion dynamics. The rows correspond to increasing tolerance levels: (top) $r = 0.1$, (middle top) $r = 0.2$, (middle bottom) $r = 0.5$, and (bottom) $r = 1.0$. The left column displays the final opinion histograms at $t = 25$, illustrating the stationary distribution of the population. The right column visualizes the temporal evolution of the opinion trajectories for a representative subset of agents.

For small tolerance levels ($r = 0.1$), shown in the top row of Figure 8, the dynamics lead to the frag-

mentation of the society. The temporal evolution (top right) reveals that agents only interact with those holding nearly identical views, causing the trajectories to run parallel without converging. Consequently, the final histogram (top left) displays a distribution broken down into multiple isolated clusters spread across the entire opinion space, maintaining a high diversity of opinions.

As the tolerance increases to intermediate values ($r = 0.2$ and $r = 0.5$), shown in the middle rows, the enhanced communication allows smaller groups to merge, however, the society still fails to reach a single global agreement. Instead, the dynamics lead to polarization, where the population splits into a few large, opposing factions. In this state, distinct groups with significantly different opinions coexist but do not merge, effectively dividing the society into separate ideological camps.

Finally, when the confidence radius is sufficiently large ($r \geq 1.0$), displayed in the bottom row, the connectivity of the society increases dramatically. Agents are open to compromising with a wider range of opinions, allowing information to propagate from the center to the extremes (bottom right). Consequently, the entire population converges toward the mean opinion ($\bar{v} \approx 0$), reaching a state of global consensus or neutrality.

In conclusion, a small increase in the confidence radius r can trigger a phase transition from a fragmented or polarized society to a state of global consensus.

6.3.2 Influence of noise (σ)

In this second experiment, we examine the impact of the stochastic diffusion parameter σ , which represents the intensity of random external influences, uncertainty in communication, or the degree of self-thinking. To analyze how noise interacts with the social tolerance level, we repeated the simulations for three specific values of the confidence radius: $r = 0.15$ (fragmentation regime), $r = 0.4$ (polarization regime), and $r = 0.8$ (consensus regime).

For each radius, we performed simulations with increasing noise levels $\sigma \in \{0.0, 0.05, 0.1, 0.15, 0.2\}$. The initial condition was a uniform distribution over $[-1, 1]$. The results are presented in Figures 9, 10, and 11, which display the final histograms and temporal evolution for increasing values of σ .

The influence of noise on the fragmentation regime ($r = 0.15$) is presented in Figure 9. In the noiseless case ($\sigma = 0$, top row), the society is characterized by fragmentation, splitting into approximately 5 to 6 isolated clusters distributed across the opinion space. However, as the noise level increases, the system undergoes a transition. The multiple small clusters disappear, giving way to a polarized state consisting of two dominant, opposing factions. Furthermore, as the noise intensity continues to increase (see bottom rows), these two groups progressively migrate toward the boundaries of the domain, resulting in a concentration of agents at the extreme opinions ($v \approx \pm 1$).

The case for the intermediate confidence radius ($r = 0.4$), shown in Figure 10, corresponds to the polarization regime. In the noiseless scenario ($\sigma = 0$, top row), the population divides into two distinct groups located symmetrically around the center. As the noise intensity σ increases, we observe that these two opinion clusters progressively move away from each other and towards the boundaries of the domain ($v = \pm 1$), similar to the $r = 0.1$ case.

Finally, Figure 11 illustrates the effect of noise on the consensus regime ($r = 0.8$). In the absence of noise ($\sigma = 0$, top row), the society reaches a state of perfect global consensus, with the entire population converging to a single opinion at the center ($v = 0$). As the noise intensity σ increases, this concentration is destabilized. The noise prevents agents from settling on a single value, causing the distribution to broaden significantly into a gaussian curve. While the population mean remains at $v \approx 0$, the increasing variance indicates that agents progressively spread out from the center, resulting in a widened distribution where agents fluctuate around the average rather than aligning perfectly.

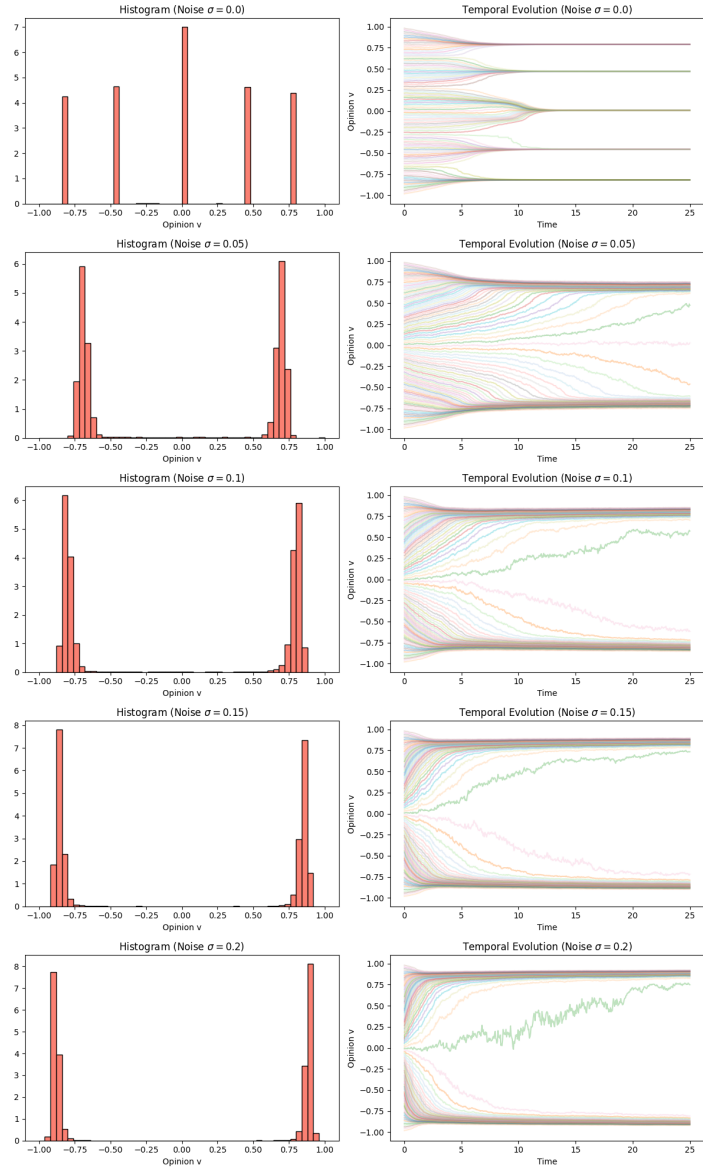


Figure 9: Influence of noise σ on the polarization regime ($r = 0.15$). The rows correspond to increasing noise levels $\sigma \in \{0.0, 0.05, 0.1, 0.15, 0.2\}$. The right column displays the histogram of the distribution at $t = 25$, and the left one displays the temporal evolution of some agents.

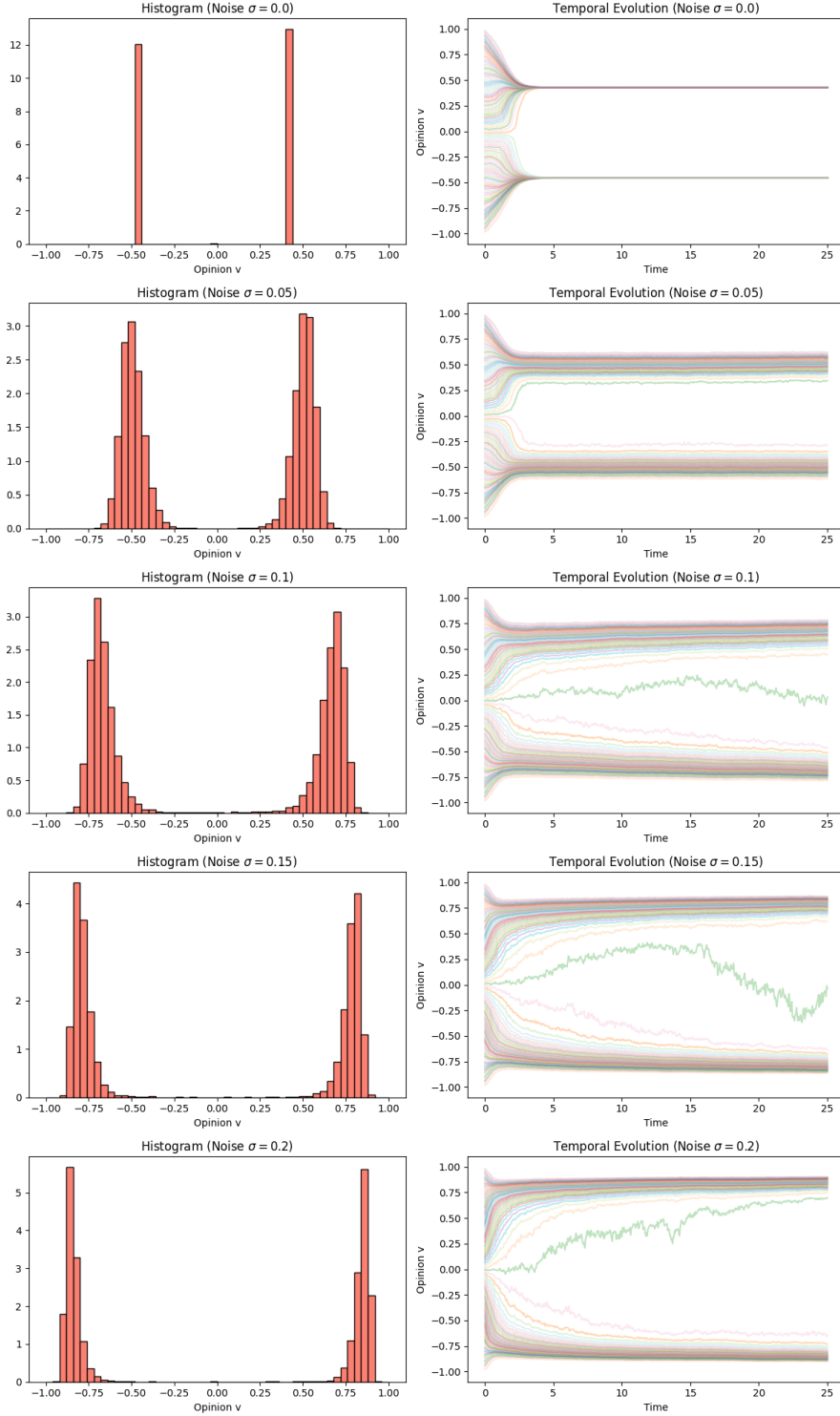


Figure 10: Influence of noise σ on the polarization regime ($r = 0.4$). The rows correspond to increasing noise levels $\sigma \in \{0.0, 0.05, 0.1, 0.15, 0.2\}$. The right column displays the histogram of the distribution at $t = 25$, and the left one displays the temporal evolution of some agents.

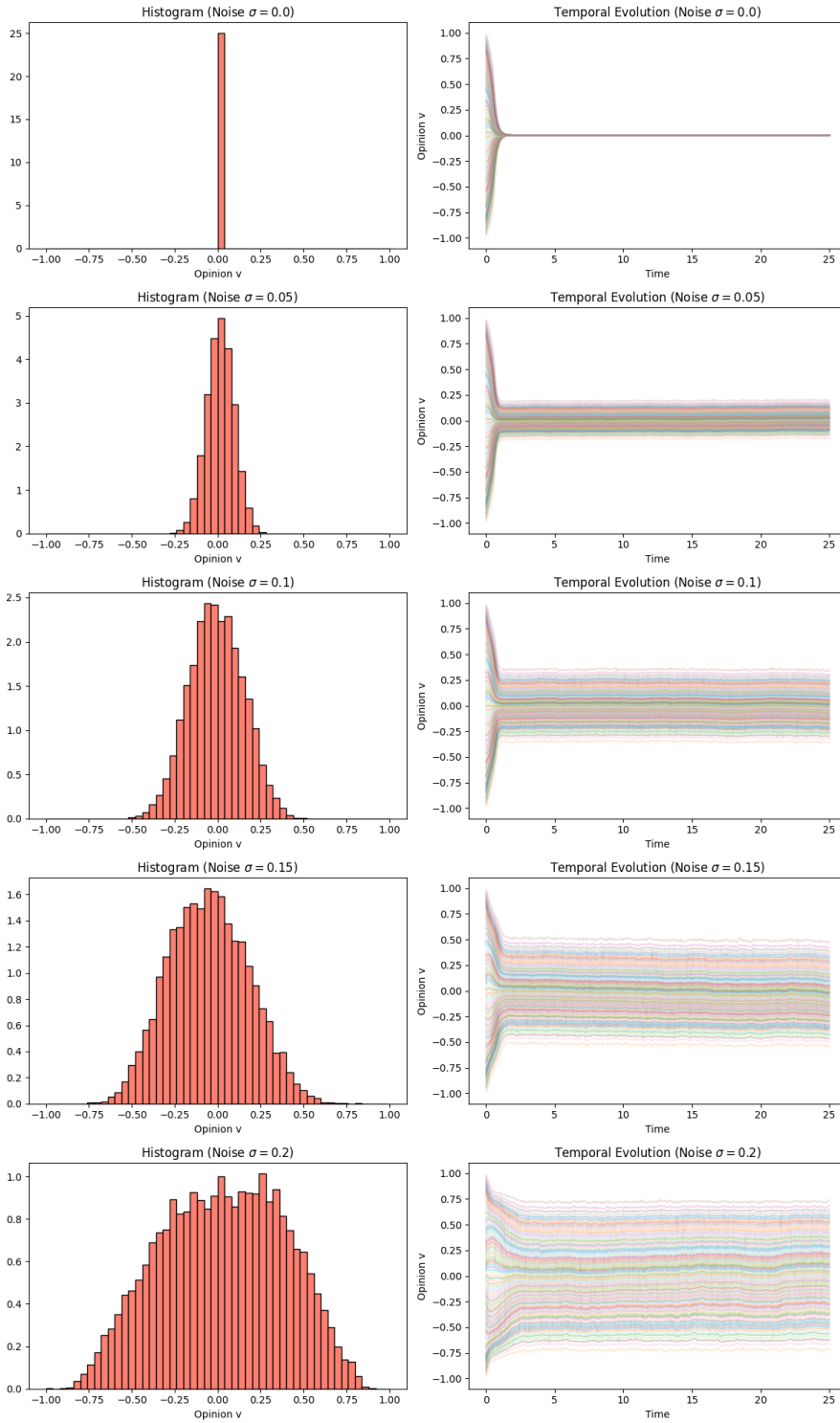


Figure 11: Influence of noise σ on the consensus regime ($r = 0.8$). The rows correspond to increasing noise levels $\sigma \in \{0.0, 0.05, 0.1, 0.15, 0.2\}$. The right column displays the histogram of the distribution at $t = 25$, and the left one displays the temporal evolution of some agents.

7. Conclusion

In this thesis, we have established a comprehensive framework connecting the microscopic dynamics of interacting agents to the macroscopic evolution of opinion distributions. We began by studying the fundamental principles of the kinetic theory of gases [14]. Starting from a system of hard spheres, we detailed the microscopic dynamics governed by elastic collisions and the Liouville equation. By applying the Boltzmann-Grad limit and the molecular chaos assumption, we formally derived the Boltzmann equation, which describes the evolution of the system. Furthermore, we demonstrated how the linear Boltzmann equation converges to the heat equation under diffusive scaling.

Building upon this theoretical basis, we transitioned from physical particles to *sociophysics* by adapting the kinetic formalism to model opinion dynamics. We introduced a “classical” model based on binary interactions and derived the corresponding Boltzmann-type equation for the evolution of opinion distributions in Section 3.1. This framework was then extended to a more realistic model in Section 3.2 that incorporates sociologically relevant parameters, specifically the compromise propensity, γ , and stochastic diffusion, σ [27]. We defined specific interaction functions, such as the local relevance of compromise P and variable diffusion D , in order to capture complex social behaviors [12].

To address the computational challenges presented by these high-dimensional integro-differential equations, we introduced Direct Simulation Monte Carlo methods. In particular, we focused on the Nanbu-Babovsky scheme and detailed its probabilistic interpretation and algorithmic implementation [2]. A significant portion of this work was dedicated to the validation of this numerical scheme [23]. By comparing our simulations against the exact analytical solution of the Kac equation, we demonstrated the accuracy and convergence of the scheme. We also analyzed the impact of time discretization and the scaling parameter ε .

We concluded by adapting the validated Nanbu-Babovsky algorithm to simulate the proposed opinion dynamics models. We introduced a modified interaction kernel to account for bounded confidence, allowing us to simulate how macroscopic phenomena such as consensus, polarization, or fragmentation emerge from the microscopic rules of agent interaction.

Finally, future steps could be done regarding opinion dynamics. We could explore different functions P and D and analyze how they influence the simulations. Additionally, a phase transition analysis could be performed to map the behavior of the simulations across different values for the confidence radius r and noise σ . Furthermore, we could improve the model by including other quantities such as assertiveness or leadership.

References

- [1] H. Babovsky. A convergence proof for nanbu's boltzmann simulation scheme. *European Journal of Mechanics. B, Fluids*, 8(1):41–55, 1989.
- [2] H. Babovsky and H. Neunzert. On a simulation scheme for the boltzmann equation. *Mathematical Methods in the Applied Sciences*, 8(1):223–233, 1986.
- [3] G. Bird. Approach to translational equilibrium in a rigid sphere gas. *Phys. Fluids*, 6:1518–1519, 1963.
- [4] G. A. Bird. *Molecular gas dynamics and the direct simulation of gas flows*. Oxford University Press, 1994.
- [5] T. Bodineau, I. Gallagher, L. Saint-Raymond, and S. Simonella. On the dynamics of dilute gases. *European Mathematical Society Magazine*, (128):13–22, 2023.
- [6] R. E. Caflisch. Monte carlo and quasi-monte carlo methods. *Acta Numerica*, 7:1–49, 1998.
- [7] J. A. Carrillo, M. Fornasier, G. Toscani, and F. Vecil. Particle, kinetic, and hydrodynamic models of swarming. In *Mathematical Modeling of Collective Behavior in Socio-Economic and Life Sciences*, pages 297–336. Springer, 2010.
- [8] C. Castellano, S. Fortunato, and V. Loreto. Statistical physics of social dynamics. *Reviews of Modern Physics*, 81(2):591–646, 2009.
- [9] C. Cercignani. The boltzmann equation. In *The Boltzmann equation and its applications*, pages 40–103. Springer, 1988.
- [10] L. Desvillettes and R. E. P. Herrera. A vectorizable simulation method for the boltzmann equation. *ESAIM: Mathematical Modelling and Numerical Analysis*, 28(6):745–760, 1994.
- [11] A. Dragulescu and V. M. Yakovenko. Statistical mechanics of money. *The European Physical Journal B-Condensed Matter and Complex Systems*, 17(4):723–729, 2000.
- [12] B. Düring, P. Markowich, J.-F. Pietschmann, and M.-T. Wolfram. Boltzmann and fokker–planck equations modelling opinion formation in the presence of strong leaders. *Proceedings of the Royal Society A: Mathematical, Physical and Engineering Sciences*, 465(2112):3687–3708, 2009.
- [13] M. Fraia and A. Tosin. The boltzmann legacy revisited: kinetic models of social interactions. *arXiv preprint arXiv:2003.14225*, 2020.
- [14] I. Gallagher. From classical mechanics to kinetic theory and fluid dynamics. *J. É. D. P. (Journées Équations aux Dérivées Partielles)*, Exposé n° II:1–14, 2014.
- [15] I. Gallagher. From classical mechanics to kinetic theory and fluid dynamics. *Journées équations aux dérivées partielles*, pages 1–14, 2014.
- [16] I. Gallagher, L. Saint-Raymond, and B. Texier. From newton to boltzmann: the case of short-range potentials. *HAL*, 2012, 2012.
- [17] M. Kac. *Probability and related topics in physical sciences*, volume 1. American Mathematical Soc., 1959.

- [18] D. P. Kroese, T. Taimre, and Z. I. Botev. *Handbook of Monte Carlo methods*. John Wiley & Sons, 2013.
- [19] N. Metropolis. The beginning. *Los Alamos Science*, 15:125–130, 1987.
- [20] N. Metropolis and S. Ulam. The monte carlo method. *Journal of the American Statistical Association*, 44(247):335–341, 1949.
- [21] K. Nanbu. Direct simulation scheme derived from the boltzmann equation. i. monocomponent gases. *Journal of the Physical Society of Japan*, 49(5):2042–2049, 1980.
- [22] National University of Singapore. Dilute gases and DSMC. https://phyweb.physics.nus.edu.sg/~phywjs/SMA_particle/MD3.pdf, 2004. Accessed: 2004-02-01.
- [23] L. Pareschi and G. Russo. An introduction to monte carlo method for the boltzmann equation. In *ESAIM: Proceedings*, volume 10, pages 35–75. EDP Sciences, 2001.
- [24] J. Peiró and S. Sherwin. Finite difference, finite element and finite volume methods for partial differential equations. In *Handbook of Materials Modeling: Methods*, pages 2415–2446. Springer, 2005.
- [25] T. Schörner-Sadenius. The Monte Carlo method: Basics and (simple) applications. <https://indico.cern.ch/event/75452/contributions/2089762/attachments/1049563/1496230/mc.pdf>, 2010. Accessed: 2010-01-28.
- [26] R. C. Tolman. The principle of microscopic reversibility. *Proceedings of the National Academy of Sciences*, 11(7):436–439, 1925.
- [27] G. Toscani. Kinetic models of opinion formation. *Commun. Math. Sci.*, 4(1):481–496, 2006.
- [28] J. Uffink and G. Valente. Lanford's theorem and the emergence of irreversibility. *Foundations of Physics*, 45(4):404–438, 2015.
- [29] T. Vicsek and A. Zafeiris. Collective motion. *Physics Reports*, 517(3-4):71–140, 2012.
- [30] J. Von Neumann. 13. various techniques used in connection with random digits. *Appl. Math Ser*, 12(36-38):3, 1951.
- [31] W. Wagner. A convergence proof for bird's direct simulation monte carlo method for the boltzmann equation. *Journal of Statistical Physics*, 66(3):1011–1044, 1992.
- [32] Wikipedia. Detailed balance — Wikipedia, the free encyclopedia. <http://en.wikipedia.org/w/index.php?title=Detailed%20balance&oldid=1329919542>, 2026. [Online; accessed 03-January-2026].
- [33] Wikipedia. Social physics — Wikipedia, the free encyclopedia. <http://en.wikipedia.org/w/index.php?title=Social%20physics&oldid=1323372118>, 2026. [Online; accessed 04-January-2026].